

A first evidence of the CMSSM is appearing soon

Yasufumi Konishi,¹ Shingo Ohta,¹ Joe Sato,¹ Takashi Shimomura,^{2,3} Kenichi Sugai,¹ and Masato Yamanaka^{4,5}

¹*Department of Physics, Saitama University, Shimo-okubo, Sakura-ku, Saitama, 338-8570, Japan*

²*Department of Physics, Niigata University, Niigata, 950-2181, Japan*

³*Max-Planck-Institut für Kernphysik, Saupfercheckweg 1, D-69117 Heidelberg, Germany*

⁴*Theory Center, Institute of Particle and Nuclear Studies,*

KEK (High Energy Accelerator Research Organization), 1-1 Oho, Tsukuba 305-0801, Japan

⁵*Department of Physics, Nagoya University, Nagoya 464-8602, Japan*

We explore the coannihilation region of the constrained minimal supersymmetric standard model (CMSSM) being consistent with current experimental/observational results. The requirements from the experimental/observational results are the 125GeV Higgs mass and the relic abundances of both the dark matter and light elements, especially the lithium-7. We put these requirements on the calculated values, and thus we obtain allowed region. Then we give predictions to the mass spectra of the SUSY particles, the anomalous magnetic moment of muon, branching fractions of the B -meson rare decays, the direct detection of the neutralino dark matter, and the number of SUSY particles produced in 14TeV run at the LHC experiment. Comparing these predictions with current bounds, we show the feasibility of the test for this scenario in near future experiment.

I. INTRODUCTION

The challenges of the LHC are to discover of the Higgs boson and to search for new physics beyond the standard model (SM). The discovery of the Higgs boson was reported by the ATLAS [1] and the CMS collaborations [2]. Meanwhile no signals of new physics have been observed so far from the LHC. However the nature indicates the existence of physics beyond the SM that accounts for the shortcomings in the SM, e.g., no candidate of dark matter, the origin of neutrino mass, the baryon asymmetry of the universe, and so on.

It is a challenge to confirm the new physics from only experimental/observational data. Theoretical studies in advance are essential to identify the signatures of new physics. We now have measurement data of the Higgs boson, the relic abundance of the dark matter, and so on. What we should do, therefore, is to precisely extract probable parameter space, and predict the signatures in each scenario of new physics by using the measurement data.

One of the leading candidates of the new physics is supersymmetric (SUSY) extension. A scenario in the extension is the constrained minimal supersymmetric SM (CMSSM) which is simple but phenomenologically successful framework [3–5]. In the CMSSM, all of the observables are described by only five parameters, and these parameters are tightly connected with the property of the Higgs boson. The reported mass of the Higgs boson, $m_h \simeq 125\text{GeV}$, suggests heavy SUSY particles [6–9]. This suggestion is consistent with a null signal of exotics at the LHC. The heavy SUSY particles imply the heavy dark matter in this framework, because the lightest SUSY particle (LSP) works as the dark matter.

Cosmological and astrophysical measurements confirmed the existence of dark matter, and numerical simulations suggest that weakly interacting massive particles (WIMPs) are the most feasible candidate for the dark matter [10–15]. In the CMSSM with R-parity conservation, the bino-like neutralino is the LSP and consequently is a WIMP dark matter candidate. The measured abundance of the neutralino dark matter can be acquired in the coannihilation region¹. The heavy neutralino dark matter requires large coannihilation rate. The large coannihilation rate sufficiently reduces the relic number density of the neutralino, and can reproduce the measured abundance of dark matter. The large coannihilation rate needs the tight degeneracy in mass between the neutralino LSP and the stau NLSP (NLSP: next to the lightest SUSY particle) [20, 21]. Indeed in large part of parameter space wherein the mass of the Higgs boson is consistent with the reported one, the mass difference between the neutralino LSP and the stau NLSP is smaller than the mass of tau lepton, m_τ [22, 23]. Such a tight degeneracy makes the stau NLSP to be long-lived charged massive particle (CHAMP) [24, 25].

The long-lived CHAMPs can modify the chain of nuclear reactions in a stage of big-bang nucleosynthesis (BBN), and hence distort the primordial abundances of light elements. The success and failure of the nucleosyn-

¹ The measured abundance is obtained also in the focus-point region in which measured abundance of dark matter can be reproduced by the large mixing of the bino and the Higgsino components [16, 17]. The latest XENON100 dark matter search, however, excludes most of parameter spaces of the focus-point region [18, 19]

thesis are quite sensitive to the property of the long-lived CHAMPs, e.g., the lifetime, the number density, the electric charge, and so on [26–57]. The success of the nucleosynthesis means to reproduce the measured abundances of light elements. Notice that measured abundance of the lithium-7 (${}^7\text{Li}$) is reported to be inconsistent with the theoretical prediction in the standard BBN; the measured one is ${}^7\text{Li}/\text{H} = 1.48 \pm 0.41 \times 10^{-10}$ [58] and the theoretical prediction is ${}^7\text{Li}/\text{H} = 5.24 \times 10^{-10}$ [59]. This inconsistency is known as the lithium-7 problem [60], and the success of the nucleosynthesis includes also solving the problem. It is important to emphasize that the success of the nucleosynthesis constrains and predicts the property of the stau NLSP.

The purpose of this work is to give theoretical clues to experimentally identify the CMSSM as the new physics in the light of the natures of the Higgs boson, the measured abundance of dark matter, and the success of the nucleosynthesis. We concentrate on the scenario wherein the mass difference of the neutralino LSP and the stau NLSP is smaller than the mass of tau lepton, and the longevity of the stau is guaranteed by the tight phase space.

Both the mass and the signal strength of the Higgs boson are correlated with parameters of the stop sector. So it sheds light on the $\text{sign}(\mu)$, m_0 , A_0 , and $\tan\beta$. The predictability of the derived relations, however, is not so strong because of too large degrees of freedom of their parameter space. Besides the property of the long-lived stau is predicted/constrained from the nucleosynthesis, and is projected mainly on the values of m_0 , A_0 , and $\tan\beta$. It should be noted that, combining the relations from the natures of the Higgs boson and the values of sfermion parameters from the BBN, as we will find, the linear relation between m_0 and A_0 are derived. Furthermore the degeneracy of the neutralino LSP and the stau NLSP in the coannihilation region set a relation between $M_{1/2}$ and sfermion parameters. Thus accumulating all of relations and constraints, we give theoretical clues on the parameter space of the CMSSM. Then we calculate the observables of terrestrial experiments based on the analysis. After the discovery of SUSY signals, by checking those with the calculation we make it possible to confirm the CMSSM in the near future.

This paper is organized as follows. In next section we recall the framework of the CMSSM, keeping an eye on the coannihilation scenario. Then we set the constraint on some input parameters from the viewpoint of the report of the Higgs boson and the observed abundances of both dark matter and light elements. In Sec. IV, we show the predictions for SUSY mass spectrum, the anomalous magnetic moment of muon, branching fractions of the B -meson rare decays, and direct detection of the neutralino dark matter in the allowed region. We show the number of the signals of the long-lived stau and the neutralino at the LHC experiment, and then we discuss the verification of the scenario in Sec V. Sec. VI is devoted to a summary and a discussion.

II. CONSTRAINTS

Here we show our constraints to derive the experimentally favored parameter space in the CMSSM.

Before we explain the detail of our constraints, we briefly review the CMSSM. The CMSSM is described by four parameters and a sign,

$$m_0, M_{1/2}, A_0, \tan\beta, \text{sign}(\mu), \quad (1)$$

where the first three parameters are the universal scalar mass, the universal gaugino mass, and the universal trilinear coupling at the scale of grand unification, respectively. Here $\tan\beta$ is the ratio of vacuum expectation values of two Higgs bosons, and μ is the supersymmetric Higgsino mass parameter. In the CMSSM, we describe all observables by these parameters, and hence we can derive the favored parameter space by putting the experimental/observational constraints on the calculated observables.

From now on, we explain in more details our constraints and how to apply those to our numerical calculations. The first requirement comes from the Higgs boson mass. The latest reports on its mass, m_h , are

$$m_h = 125.8 \pm 0.4(\text{stat}) \pm 0.4(\text{syst}) \text{ GeV}, \quad (2)$$

by the CMS collaboration [61], and

$$m_h = 125.2 \pm 0.3(\text{stat}) \pm 0.6(\text{syst}) \text{ GeV}, \quad (3)$$

by the ATLAS collaboration [62], respectively. It is known that the Higgs boson mass calculated by each public codes fluctuates by about $\pm 3\text{GeV}$ [63–66]. Taking into account these uncertainties, we apply a more conservative constraint as

$$m_h = 125.0 \pm 3.0 \text{ GeV}. \quad (4)$$

The second constraint comes from the observation for the relic abundance of the dark matter. The WMAP satellite reported the value at the 3 sigma level [15],

$$0.089 \leq \Omega_{\text{DM}} h^2 \leq 0.136. \quad (5)$$

In most of the CMSSM parameter space, the relic abundance of the neutralino LSP is over-abundant against the measured value. The correct dark matter abundance requires the unique parameter space where the bino-like neutralino LSP and the stau NLSP are degenerate in mass so that the coannihilation mechanism works well [20, 21].

The third and fourth constraints are required from solving the lithium-7 problem. The stau NLSP is long-lived if the mass difference is smaller than the mass of tau lepton [24, 25]. In the case that the stau survives until the BBN epoch, the lithium-7 density can be reduced to the measured value with the exotic nuclear reactions induced by the stau. As the third condition, we impose the mass difference, δm , to be

$$\delta m \equiv m_{\tilde{\tau}_1} - m_{\tilde{\chi}_1^0} \leq 0.1\text{GeV}, \quad (6)$$

where $m_{\tilde{\tau}_1}$ and $m_{\tilde{\chi}_1^0}$ are the masses of the stau NLSP and the neutralino LSP, respectively. With this mass difference, the stau NLSP is sufficiently long-lived so that it can survive until the BBN era [36, 49, 54]. In our numerical calculation, we use the pole mass of top quark as an input which involves an uncertainty of $\mathcal{O}(1)\text{GeV}$. It is expected that the SUSY spectrum also includes the same order of uncertainties. So in the numerical results in the next section, we show also the case of

$$\delta m \leq 1 \text{ GeV}, \quad (7)$$

to make more conservative prediction on the CMSSM parameters².

The forth constraint is the upper bound on the mass of the neutralino LSP,

$$m_{\tilde{\chi}_1^0} \leq 450 \text{ GeV}. \quad (8)$$

This upper bound is derived from the requirement of the abundances of both the dark matter and light elements. The yield value of the negatively charged stau at the BBN epoch is required to be larger than $Y_{\tilde{\tau}_1}^{\text{BBN}} \gtrsim 1.0 \times 10^{-13}$, where $Y_{\tilde{\tau}_1} = n_{\tilde{\tau}_1}/s$ (s is the entropy density), to sufficiently reduce the lithium-7 [54]. Assuming the enough longevity of the stau, $Y_{\tilde{\tau}_1}^{\text{BBN}}$ is fixed at when the ratio of number densities of the stau NLSP and the neutralino LSP are frozen out. The yield value $Y_{\tilde{\tau}_1}^{\text{BBN}}$ is expressed with the relic density of the neutralino dark matter $Y_{\tilde{\chi}_1^0}^{\text{relic}}$

$$Y_{\tilde{\tau}_1}^{\text{BBN}} = \frac{Y_{\tilde{\chi}_1^0}^{\text{relic}}}{2(1 + e^{\delta m/T_f})}. \quad (9)$$

Here T_f is the freeze-out temperature of the ratio, $T_f \simeq (m_{\tilde{\tau}_1} - \delta m)/25$. The relic abundance of the dark matter is bounded (see Eq. (10)),

$$\Omega_{\text{DM}} h^2 \equiv \frac{Y_{\tilde{\chi}_1^0}^{\text{relic}} s_0 m_{\text{DM}} h^2}{\rho_c} \leq 0.136. \quad (10)$$

Here s_0 is the today's entropy density, h is the scale factor of the Hubble expansion rate, and ρ_c is the critical density. Combining these facts, we obtain the upper bound on the mass of the neutralino dark matter,

$$m_{\tilde{\chi}_1^0} \lesssim \frac{\rho_c}{2s_0 h^2 (1 + e^{\delta m/T_f})} \frac{0.136}{1.0 \times 10^{-13}}. \quad (11)$$

Hence the upper bound on the neutralino mass is $m_{\tilde{\chi}_1^0} \leq 450 \text{ GeV}$.

III. ALLOWED REGION IN THE CMSSM

In this section, we show the allowed region in the CMSSM parameter space by imposing the constraints explained in Sec. II. We calculate the SUSY spectrum, the DM abundance and other observables using micrOMEGAs [67] implementing SPheno [68, 69], and the lightest Higgs mass using FeynHiggs [70–73].

A. A_0 - m_0 plane

In Fig. 1, we show the allowed region in m_0 - A_0 plane for $\tan \beta = 10, 20$, and 30 from top to bottom and $\delta m \leq 1$ and 0.1 GeV from left to right panels, respectively. Color represents $M_{1/2}$.

Notably, one can see that A_0 and m_0 have an almost linear relation for fixed $M_{1/2}$. The relations can be parameterized as

$$m_0 = -5.5 \times 10^{-3} A_0 \tan \beta + b, \quad (12)$$

$$b \simeq \begin{cases} (122, 190) \text{ GeV} & \text{for } \tan \beta = 10, \\ (165, 228) \text{ GeV} & \text{for } \tan \beta = 20, \\ (225, 283) \text{ GeV} & \text{for } \tan \beta = 30. \end{cases}$$

These linear relations come from the tight degeneracy in mass between the stau and the neutralino. We explain the linear relation as follows. Firstly we note that signs of μ and A_0 is opposite each other due to obtaining the large Higgs boson mass as we explain latter. In this scenario we choose $\mu > 0$ and $A_0 < 0$, respectively. For a fixed $m_{\tilde{\chi}_1^0}$, in response to an increasing of m_0 , the mass of the lighter stau is also increased. In order to keep the mass difference to be smaller than 1 GeV (0.1 GeV), $|A_0|$ also has to be increased. Increasing of $|A_0|$ makes a non-diagonal element of the stau mass matrix to be large, and hence the mass eigenvalue of the lighter stau is decreased after diagonalization to be within the small mass difference. As a result, the linear behavior in the A_0 - m_0 plane is found.

One can see in Fig. 1 that m_0 in the allowed region increases as $\tan \beta$ increases. This is because the soft masses of the staus are more decreased for larger $\tan \beta$ in RG running due to the tau Yukawa couplings. The terms with tau Yukawa coupling in RGE decrease the soft masses in the running [74]. These become significant when $\tan \beta$ is large because the tau Yukawa coupling is proportional to $1/\cos \beta$. Thus larger m_0 is required for larger $\tan \beta$ to obtain the stau mass satisfying with Eq.(6) or (7).

The upper and the lower edges of the allowed region in all panels of the Fig. 1 are determined by the constraints of the correct abundances both of the dark matter and the light elements. This can be understood as follows. Since the dark matter abundance is depend on the neutralino LSP mass as shown in Eq. (10), the dark matter abundance gives the lower bound on the neutralino mass. On the other hand, the light elements abundance gives

² In a precise sense, a too small mass difference makes the stau too long lived. If the stau lives long sufficient to form a bound state with a helium, the stau converts it another nuclei, a deuteron and a triton. Those reactions make number densities of converted nuclei too large compared with those of observations [54]. Number densities of these nuclei therefore become inconsistent with observed values through those reactions and too small mass difference is not allowed. This is, however, considerably relaxed by introducing a tiny lepton flavor violation [56].

the upper bound as shown in Eq. (8). The bounds for the lighter stau mass is nearly same as that for the neutralino mass due to the tight degeneracy. Therefore once A_0 is fixed, m_0 can vary in range satisfying the bound for the lighter stau mass. Thus, the upper and the lower edges are determined by the constraints.

On the other hand, the right side of the allowed region is determined by the lower bound on the Higgs boson mass. We can see from the the left panel of Fig. 2 that the Higgs boson mass reaches to 122GeV. The mass square of the Higgs boson with one-loop corrections is given by

$$m_h^2 = m_Z^2 \cos^2 2\beta + \frac{3m_t^4}{16\pi^2 v^2} \left[\log \left(\frac{m_t^2}{m_{\tilde{t}}^2} \right) + \frac{X_t^2}{m_{\tilde{t}}^2} \left(1 - \frac{X_t^2}{12m_{\tilde{t}}^2} \right) \right], \quad (13)$$

$$(X_t = A_t - \mu \cot \beta, \quad m_{\tilde{t}} = \sqrt{m_{\tilde{t}_1} m_{\tilde{t}_2}}),$$

where the first line represents the tree-level mass square and the second one is the one-loop corrections [6–9]. The tree-level contribution is simply given by the Z boson mass m_Z while the radiative corrections are given by the masses of the top m_t , the lighter/heavier stop $m_{\tilde{t}_1/\tilde{t}_2}$, the stop mixing parameter X_t , and the vacuum expectation values of the Higgs bosons, $v = \sqrt{v_u^2 + v_d^2}$, here v_u and v_d are vacuum expectation values of up-type and down-type Higgs boson, respectively. The radiative corrections are sensitive to the stop mixing parameter. As is well known, the second term in the bracket decreases quadratically from its maximum at

$$|X_t| = \sqrt{6}m_{\tilde{t}}. \quad (14)$$

To obtain maximum value of $|X_t|$, signs of μ and A_0 have to be opposite each other, and we choose $\mu > 0$ and $A_0 < 0$ in this paper. The right panel of Fig. 2 shows $|X_t|/\sqrt{6}m_{\tilde{t}}$ in the allowed region for $\tan \beta = 20$ and $\delta m \leq 1\text{GeV}$. It can be seen that $|X_t|$ is smaller than $\sqrt{6}m_{\tilde{t}}$ at the right side edge, and hence the one-loop corrections are not so large that m_h is pushed up to the lower bound. Similarly, the left side edge is also determined by the Higgs boson mass bound. The value of $|X_t|/\sqrt{6}m_{\tilde{t}}$ gradually becomes large as $|A_0|$ increases. At a large $(|A_0|, m_0)$ point, the value of $|X_t|/\sqrt{6}m_{\tilde{t}}$ is equal to 1, and therefore m_h receives the maximal loop correction. In the region where $|X_t|/\sqrt{6}m_{\tilde{t}} > 1$, the loop corrections to m_h are smaller and m_h decreases from the maximal value. Therefore m_h is smaller than 122GeV again at the left side edge as can be seen in the right panel of Fig. 2.

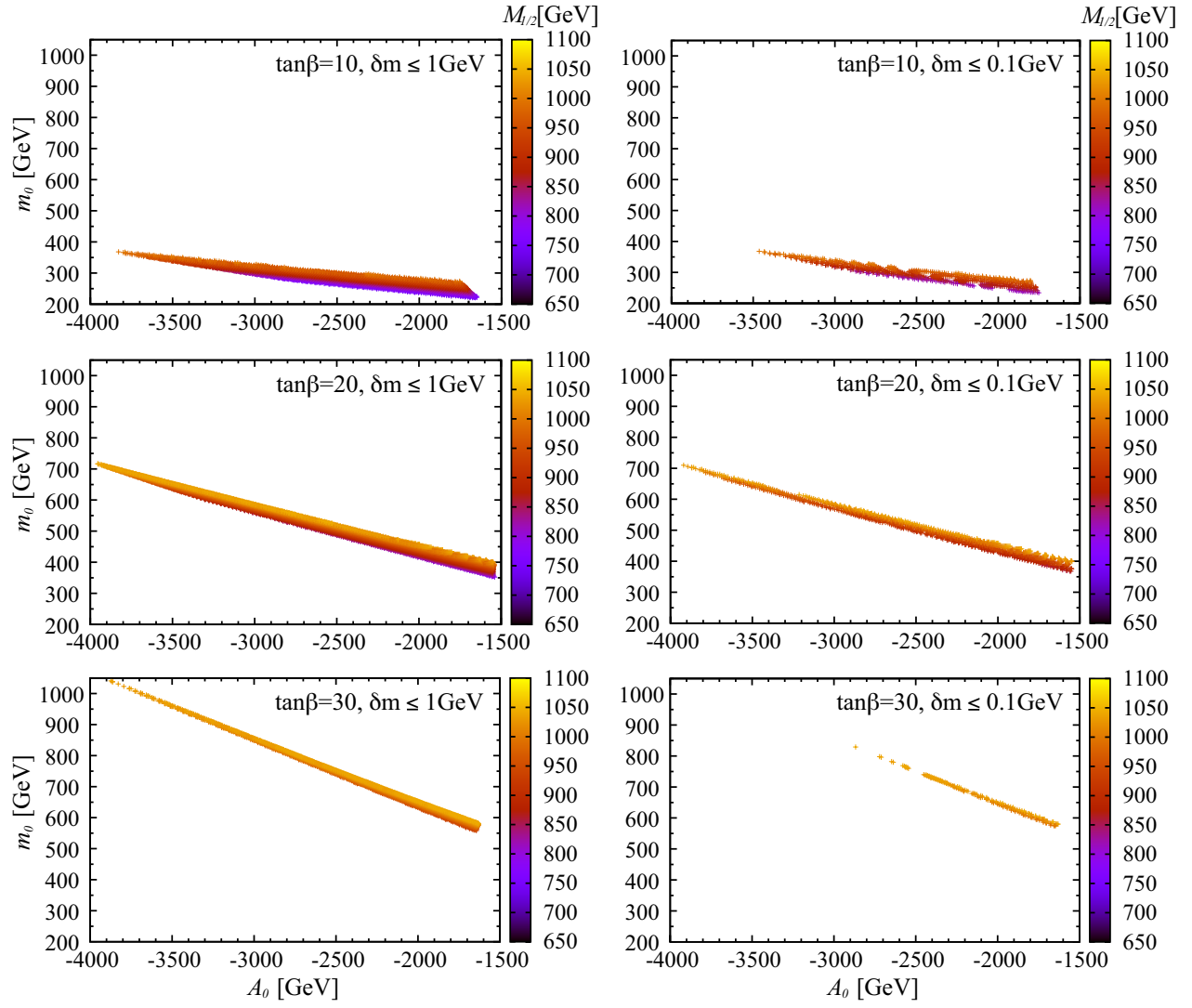


FIG. 1: Allowed region in A_0 - m_0 plane. We fix $\tan\beta$ to 10, 20 and 30 from top to bottom and $\delta m \leq 1$ and 0.1 GeV from left to right. A gradation of colors represents $M_{1/2}$. Light color indicates large value, and dark color indicates small value.

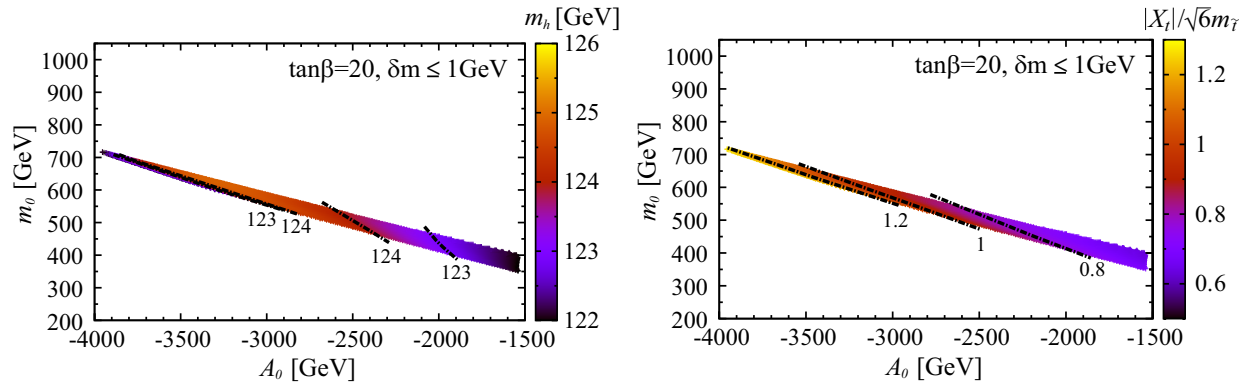


FIG. 2: Left panel: the value of the Higgs boson mass. Right panel: the ratio of $|X_t|$ to $\sqrt{6}m_{\tilde{t}}$. A gradation of colors represents each value. Light color indicates large value, and dark color indicates small value. We fix $\tan\beta$ to 20 and $\delta m \leq 1$ GeV in each figure.

B. $m_0 - M_{1/2}$ plane

We show in Fig. 3 the allowed region in m_0 - $M_{1/2}$ plane for $\tan\beta = 10, 20$ and 30 from top to bottom and $\delta m \leq 1$ and 0.1GeV from left to right panels, respectively. Color and the contours represents A_0 . Figure 4 shows the Higgs boson mass in the left panel and the relic abundance of the dark matter in the right panel by color on the allowed region. We fix $\tan\beta$ to 20 and $\delta m \leq 1\text{GeV}$ in the panels.

In Fig. 3, it can be seen that $|A_0|$ is larger as m_0 is larger while it is slightly dependent on $M_{1/2}$. This is because the lighter stau mass is mainly determined by m_0 and A_0 as is explained in Sec. III A. In the figure, we obtain $m_h \simeq 126\text{GeV}$, at $(m_0, M_{1/2}) = (350, 1000)\text{GeV}$ for $\tan\beta = 10$, $(640, 1050)\text{GeV}$ for $\tan\beta = 20$, and $(800, 1050)\text{GeV}$ for $\tan\beta = 30$, respectively. These points are located at the middle of m_0 and the upper edge of $M_{1/2}$ in the allowed region. The value of $|X_t|$ is equal to $\sqrt{6}m_{\tilde{t}}$ at these points, and hence m_h receives the large loop corrections. Furthermore the logarithmic term in Eq. (13) becomes large as $M_{1/2}$ increases since the stops become heavy as we show later in Fig. 6. Thus, the Higgs boson mass is pushed up to 126GeV . The Higgs boson mass decreases as the parameters deviate from these points. In the left panel of Fig. 4, it is clearly seen that the lower bound on the Higgs boson mass determines the left and the right edges in the allowed region. Since $|A_0|$ is small at the left edge, the value of $|X_t|$ is smaller than $\sqrt{6}m_{\tilde{t}}$. Therefore m_h receives a small one-loop correction. On the contrary, $|A_0|$ is large at the right edge, and $|X_t|$ is larger than $\sqrt{6}m_{\tilde{t}}$. It means that m_h receives a small one-loop correction as we explained in the previous subsection.

Note that the minimum value of $M_{1/2}$ in the allowed region are different in each panel. The minimum value is determined by the lower bound on the relic abundance of the dark matter. In the right panel of Fig. 4, we can see that the neutralino relic abundance reaches to the lower bound at the bottom edge of the allowed region³. The minimum value of $M_{1/2}$ becomes large as $\tan\beta$ increases and/or the mass difference becomes small.

The $\tan\beta$ dependence on the relic abundance is understood as follows. In the favored parameter region, the stau NLSP consists mostly of the right-handed stau. Then the dominant contribution to the total coannihilation rate of the dark matter is the stau-stau annihilation into tau leptons via Higgsino exchange for large $\tan\beta$ [75]. The interactions of the stau-tau lepton-Higgsino is proportional to $\tan\beta$, and so the large $\tan\beta$ leads the large coannihilation rate of the dark matter.

Larger $\tan\beta$ therefore makes the relic abundance to be smaller.

The dependence of the relic number density on the mass difference is understood in terms of the ratio of number density of the stau to the neutralino. At the freeze out of total number of all of SUSY particles, the ratio is proportional to $e^{-\delta m/T_f^{\text{total}}}$. Since the freeze out temperature T_f^{total} is almost the same for $\delta m = 0.1$ and 1GeV as long as $m_{\tilde{\chi}_1^0}$ is fixed, the stau number density is relatively large for $\delta m = 0.1\text{GeV}$. This leads that the total coannihilation rate become enlarged and hence the relic number density of the neutralino is reduced. Such reduction of the number density can be compensated by increasing the neutralino mass. Thus, the minimum value of $M_{1/2}$ should be larger for larger $\tan\beta$ and smaller δm to meet the lower bound for the dark matter abundance.

On the other hand, the maximum value of $M_{1/2}$ is fixed from the upper bound in Eq. (8). Note that the upper bound is derived by the fact that the large number density of the stau is required to reduce the lithium-7 to be the measured abundance. This requirement forbids too large mass of the neutralino. As there is a relation between the neutralino mass and $M_{1/2}$, i.e., $m_{\tilde{\chi}_1^0} \simeq 0.43M_{1/2}$, the upper bound of $M_{1/2}$ is estimated by the neutralino mass, and is fixed to be 1TeV in the present paper.

We emphasize here that the maximum value of $M_{1/2}$ in the allowed region is unique in the parameter space. If we do not take into account the lithium-7 problem, heavier neutralino or $M_{1/2}$ is allowed, and hence the resultant range of $M_{1/2}$ is wider.

³ In the panel, we see moderate stripes on the allowed region. These stripes result from the low accuracy of the numerical calculation. We are not able to collect all data with the mass difference within 0.1GeV . If we collect all data, these stripes are not on the allowed region.

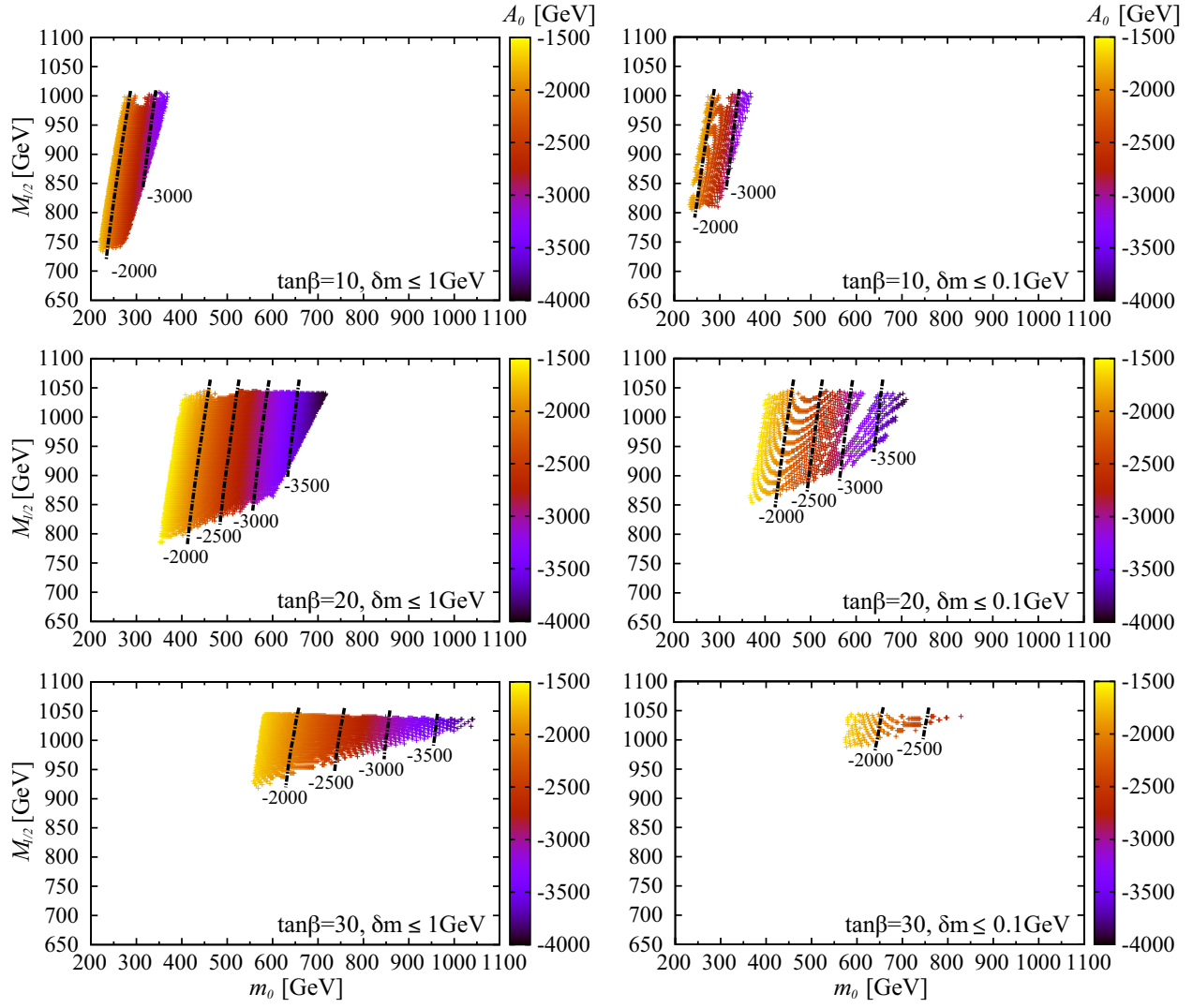


FIG. 3: Allowed parameter region in m_0 - $M_{1/2}$ plane. We fix $\tan\beta$ to 10, 20 and 30 from top to bottom and $\delta m \leq 1$ and 0.1 GeV from left to right, respectively. A gradation of colors represents A_0 . Light color indicates large value, and dark color indicates small value.

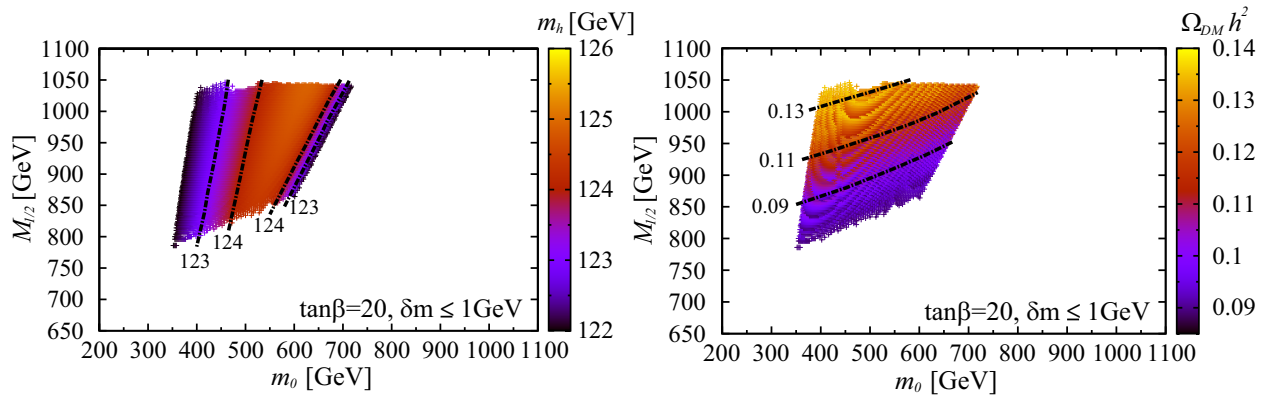


FIG. 4: Left panel: the value of the Higgs boson mass. Right panel: the value of the relic abundance of the dark matter. A gradation of colors represents each value. Light color indicates large value, and dark color indicates small value. We fix $\tan\beta$ to 20 and $\delta m \leq 1$ GeV in each figure.

IV. SUSY SPECTRUM, $(g-2)_\mu$, B MESON RARE DECAYS AND DARK MATTER DETECTION

In this section, we show our predictions on the SUSY spectrum, the muon anomalous magnetic moment, rare decays of B mesons, and the dark matter direct detections. We calculate mass spectrum of SUSY particles by using SPheno [68, 69] and that of Higgs boson by using FeynHiggs [70–73].

A. Spectra of SUSY particles with current limits

We show the mass spectra of SUSY particles in the allowed region. Figure 5 shows the masses of the gluino, the first and the second generations squarks with respect to the lightest neutralino mass, respectively. From top to bottom, $\tan\beta$ is varied with 10, 20 and 30, and in the left and the right panels $\delta m \leq 1$ and 0.1 GeV. Similarly the masses of the stop and sbottom are shown in Fig. 6, those of the neutralino, the slepton and the heavier Higgs in Fig. 7, Fig. 8 and in Fig. 9, respectively. Note that in all of figures we have excluded the region with $m_{\tilde{\chi}_1^0} (\simeq m_{\tilde{\tau}_1}) \lesssim 339$ GeV, which is the direct bound on the long-lived CHAMP at the LHC [76]. We explain behaviors of these figures in following subsections.

1. Gluino, neutralinos and heavy Higgs boson masses

In the CMSSM, the gluino mass parameter M_3 is related to the bino and the wino mass parameter M_1 and M_2 at one-loop RGE as follows,

$$M_3 = \frac{\alpha_s}{\alpha} \sin^2 \theta_W M_2 = \frac{3}{5} \frac{\alpha_s}{\alpha} \cos^2 \theta_W M_1. \quad (15)$$

From this relations, we can obtain the ratio

$$M_3 : M_2 : M_1 \simeq 6 : 2 : 1, \quad (16)$$

around the TeV scale. We can see that $m_{\tilde{g}}$ is nearly 6 times larger than $m_{\tilde{\chi}_1^0}$ in Fig. 5, and $m_{\tilde{\chi}_2^0}$ is about twice as large as that in Fig. 7. This means that the second lightest neutralino is almost the neutral wino. On the other hand, $m_{\tilde{\chi}_3^0}$ and $m_{\tilde{\chi}_4^0}$ extend above 1 TeV because these consist of the neutral Higgsinos. Their masses are given by μ parameter that is sensitive to m_0 for fixed $m_{\tilde{\chi}_1^0}$. The modulus $|\mu|$ is determined by the EWSB conditions. At tree level the corresponding formula for the correct EWSB leads as

$$|\mu|^2 = \frac{1}{2} [\tan 2\beta (M_{H_u}^2 \tan \beta - M_{H_d}^2 \cot \beta) - m_Z^2]. \quad (17)$$

where M_{H_d} and M_{H_u} are the down-type and the up-type Higgs soft SUSY breaking masses. For $\tan \beta \gg 1$, Eq. (17) is approximated as follows

$$|\mu|^2 \simeq -M_{H_u}^2. \quad (18)$$

The soft mass $M_{H_u}^2$ is sensitive to m_0 . The approximate solution of the one-loop RGE for $M_{H_u}^2$ is given by

$$m_{H_u}^2 \simeq -3.5 \times 10^3 \cot^2 \beta m_0^2 + 87 \cot \beta M_{1/2} m_0' - 2.8 M_{1/2}^2, \quad (19)$$

where $m_0' \equiv m_0 - b$, and b is defined in Eq. (12). Therefore $m_{\tilde{\chi}_3^0}$ and $m_{\tilde{\chi}_4^0}$ become large with increasing m_0 .

Meanwhile, the mass of the CP-odd Higgs boson, m_A , is given by,

$$m_A^2 \simeq |\mu|^2. \quad (20)$$

Thus, the masses of the heavy Higgs boson and the CP-odd Higgs boson are determined by $|\mu|$, and these are close to $m_{\tilde{\chi}_3^0}$ and $m_{\tilde{\chi}_4^0}$ as is shown in Figs. 7 and 9.

2. First and Second generation squarks, sleptons masses

For the first and the second generation squarks and sleptons, the effects of the corresponding Yukawa couplings are negligible in RG evolutions of their soft masses. The soft SUSY breaking masses are parameterized up to the one-loop order as [74],

$$m_{\tilde{q}_L}^2 \simeq m_0^2 + 4.7 M_{1/2}^2, \quad (21a)$$

$$m_{\tilde{q}_R}^2 \simeq m_0^2 + 4.3 M_{1/2}^2, \quad (21b)$$

$$m_{\tilde{e}_L}^2 \simeq m_0^2 + 0.5 M_{1/2}^2, \quad (21c)$$

$$m_{\tilde{e}_R}^2 \simeq m_0^2 + 0.1 M_{1/2}^2. \quad (21d)$$

Note that the slepton masses are sensitive to m_0 in Fig. 8 while the squark masses are insensitive to m_0 in Fig. 5. In Eqs. (21a) and (21b) the second term is dominant, and hence we approximate these equations more roughly as follows:

$$\begin{aligned} m_{\tilde{q}_L} &\simeq 2.2 M_{1/2}, \\ m_{\tilde{q}_R} &\simeq 2.1 M_{1/2}. \end{aligned} \quad (22)$$

Meanwhile, in Eqs. (21c) and (21d) the contributions to soft mass from the first term is comparable to that of the second term. Therefore, the slepton masses are sensitive to m_0 .

3. Stop mass spectra

Figure 6 shows the masses of the stops. Unlike in the case of the other sfermions, the distributions of stop masses are in nonlinear relation. The spread of the distributions in the lightest neutralino mass-stop mass plane is understood as follows.

The masses of the stops in mass eigenstate are given

by

$$m_{\tilde{t}_1, \tilde{t}_2}^2 \simeq \frac{1}{2} (m_{Q_3}^2 + m_{U_3}^2) \mp \frac{1}{2} \sqrt{(m_{Q_3}^2 - m_{U_3}^2)^2 + 4(m_{\tilde{t}_{LR}}^2)^2}, \quad (23a)$$

$$m_{\tilde{t}_{LR}}^2 = m_t(A_t - \mu \cot \beta), \quad (23b)$$

where m_{Q_3} and m_{U_3} are the soft SUSY breaking masses, and A_t is the stop trilinear coupling. In Eq. (23a) the first term is dominant, and it is a decreasing function of m_0^2 because of the top and bottom Yukawa couplings. Meanwhile, the second term in Eq. (23a) is an increasing function of m_0^2 . This is because the dominant term in the square root is $m_{\tilde{t}_{LR}}^2$ involving A_t , and the coupling A_t is proportional to m_0 due to the relation between A_0 and m_0 in Eq. (12). Hence, for a fixed lightest neutralino mass, stop masses are not simply determined as a function of the lightest neutralino mass, and rather spread depending on the m_0^2 .

The ATLAS collaboration gives the bound for the stop mass from the direct stop search at 8 TeV LHC run [77]. Note that our results of the stop mass are safely above the bound.

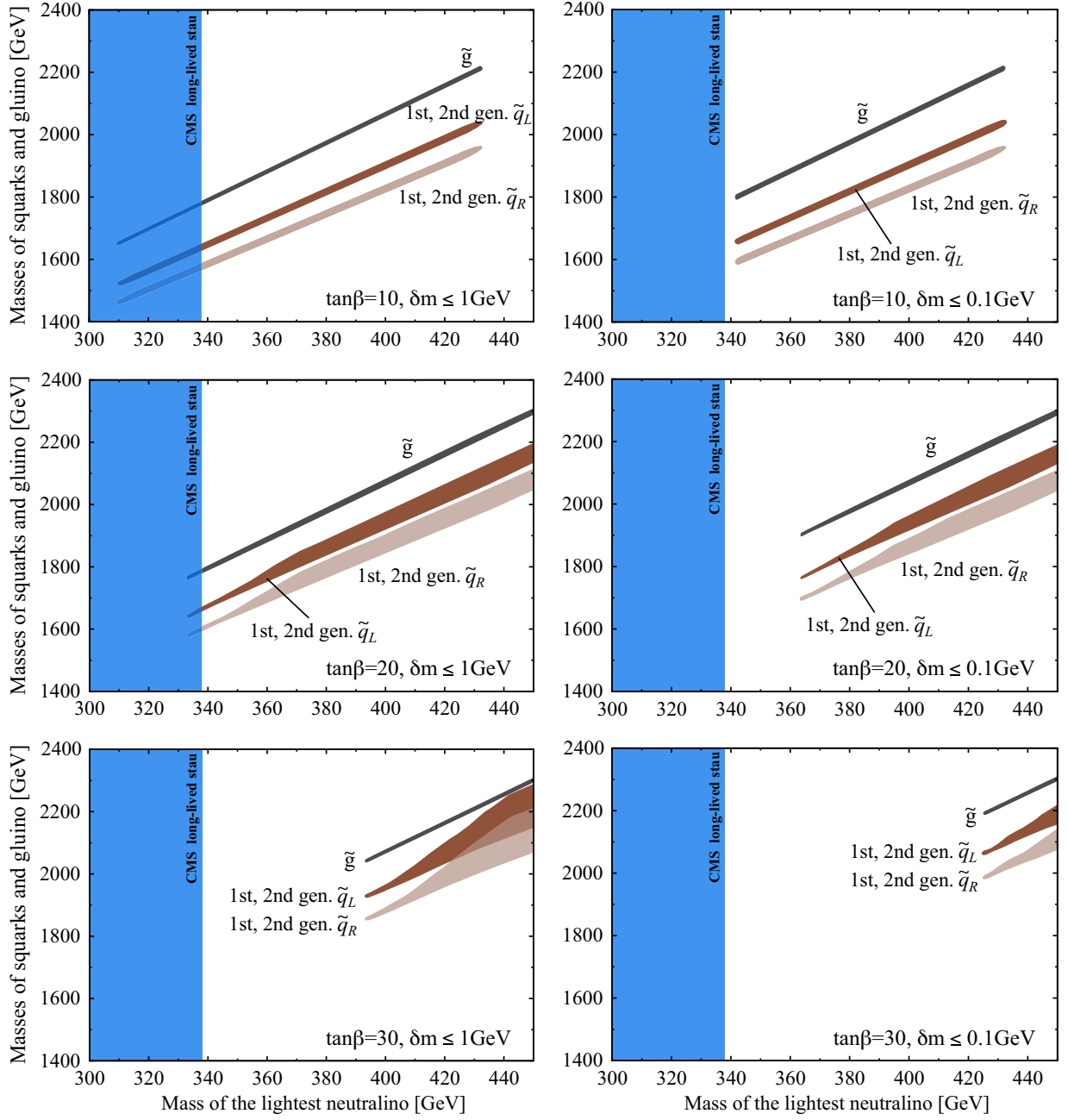


FIG. 5: Mass spectra of the gluino and the first and second generations squarks. The horizontal axis represents the mass of the LSP neutralino. We fix $\tan\beta$ to 10, 20 and 30 from top to bottom and $\delta m \leq 1$ and 0.1 GeV from left to right, respectively.

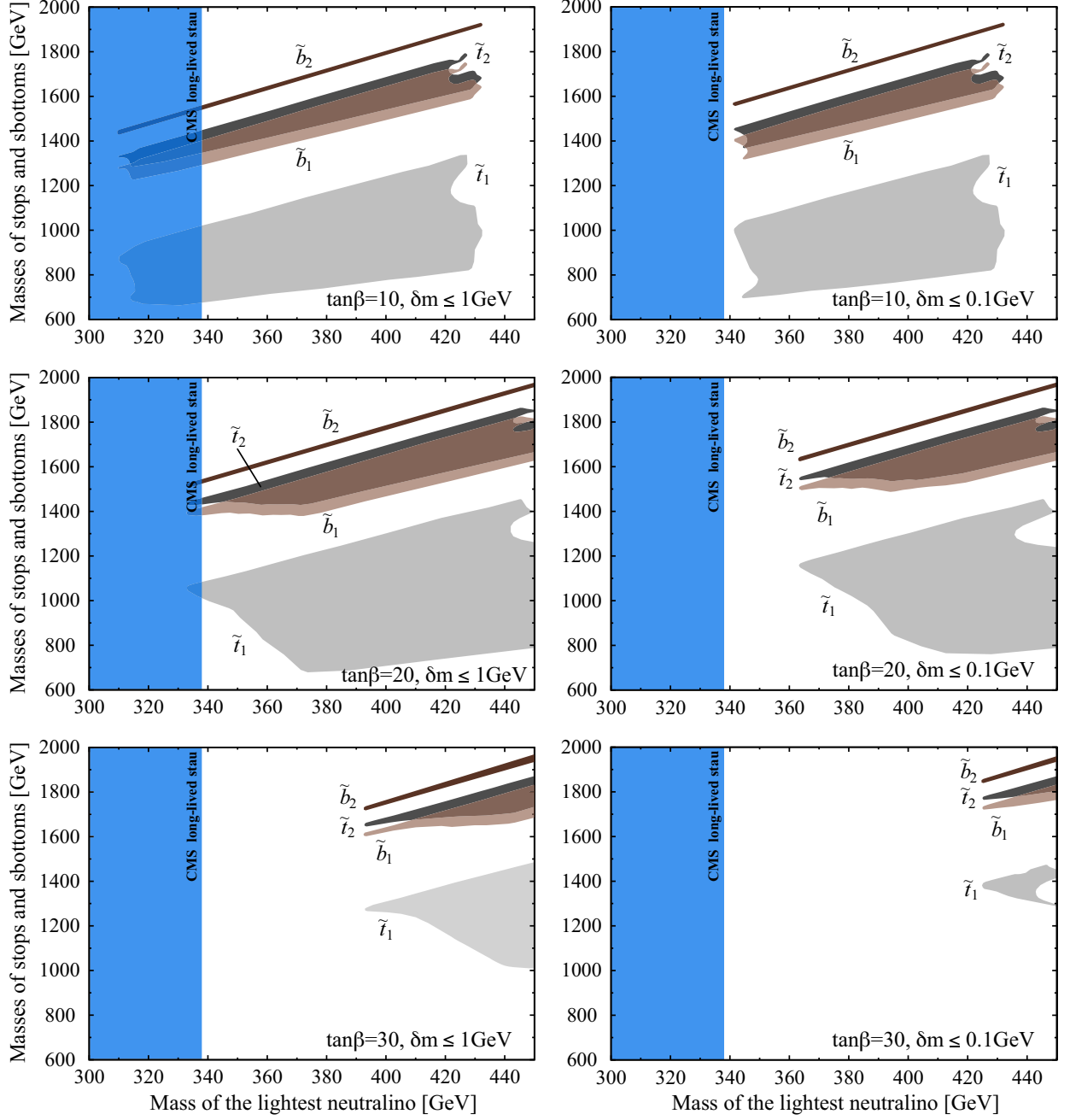


FIG. 6: Mass spectra of the stop and the sbottom. The horizontal axis expresses the mass of the LSP neutralino. We fix $\tan\beta$ to 10, 20 and 30 from top to bottom and $\delta m \leq 1$ and 0.1 GeV from left to right, respectively.

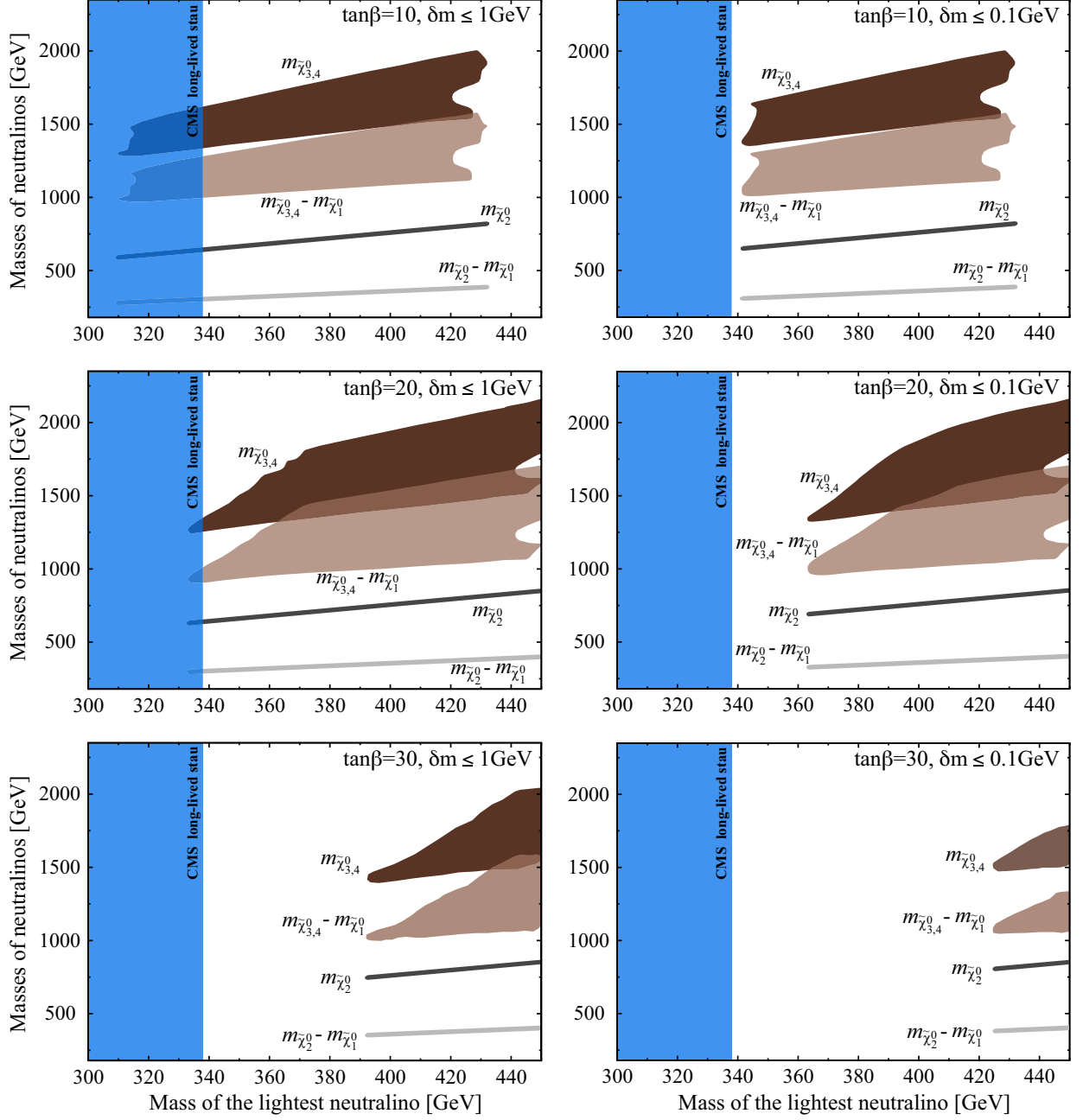


FIG. 7: Mass spectra of the neutralino. The horizontal axis represents the mass of the LSP neutralino. We fix $\tan\beta$ to 10, 20 and 30 from top to bottom and $\delta m \leq 1$ and 0.1 GeV from left to right, respectively.

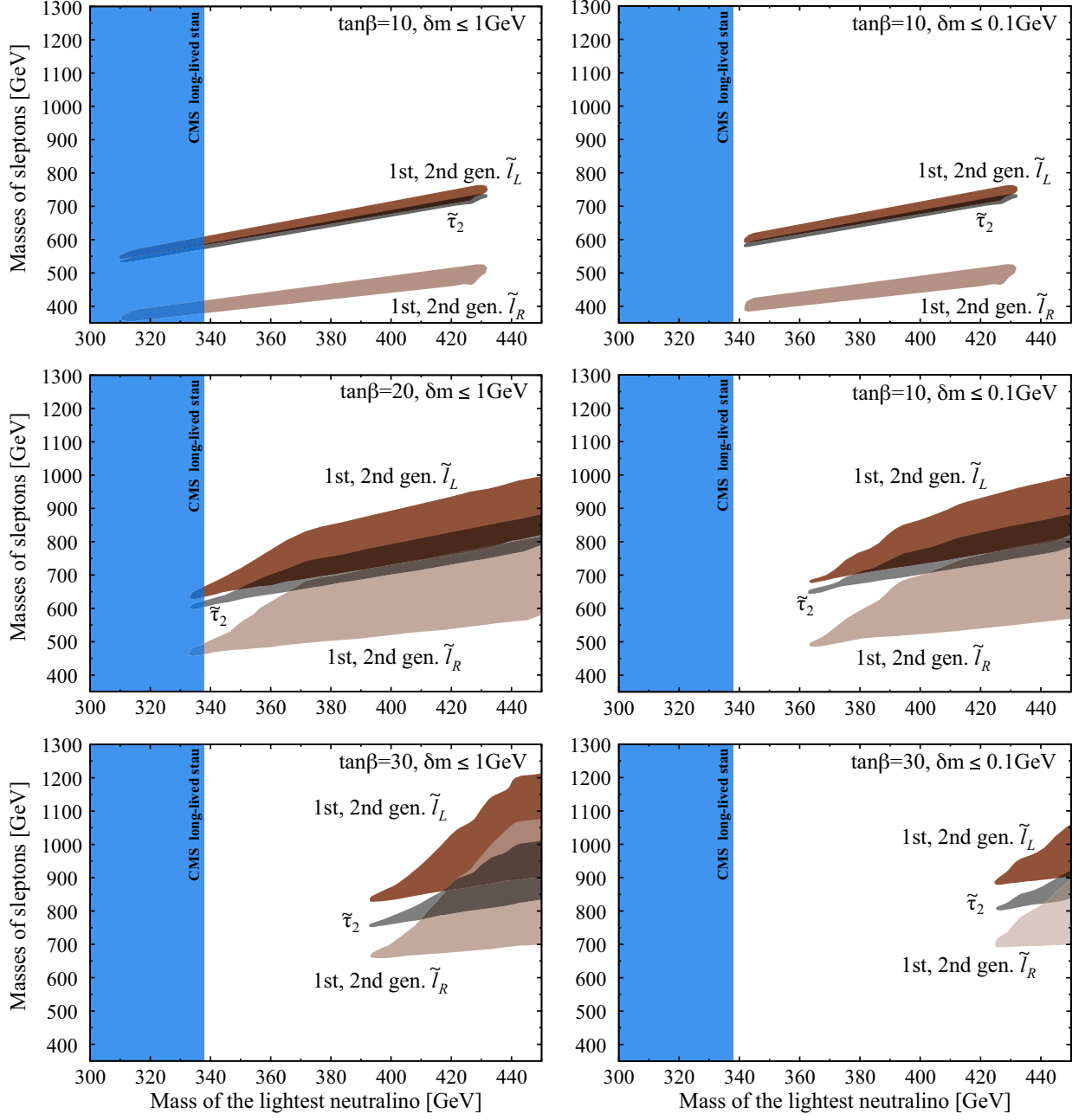


FIG. 8: Mass spectra of the slepton. The horizontal axis represents the mass of the LSP neutralino. We fix $\tan\beta$ to 10, 20 and 30 from top to bottom and $\delta m \leq 1$ and 0.1 GeV from left to right, respectively.

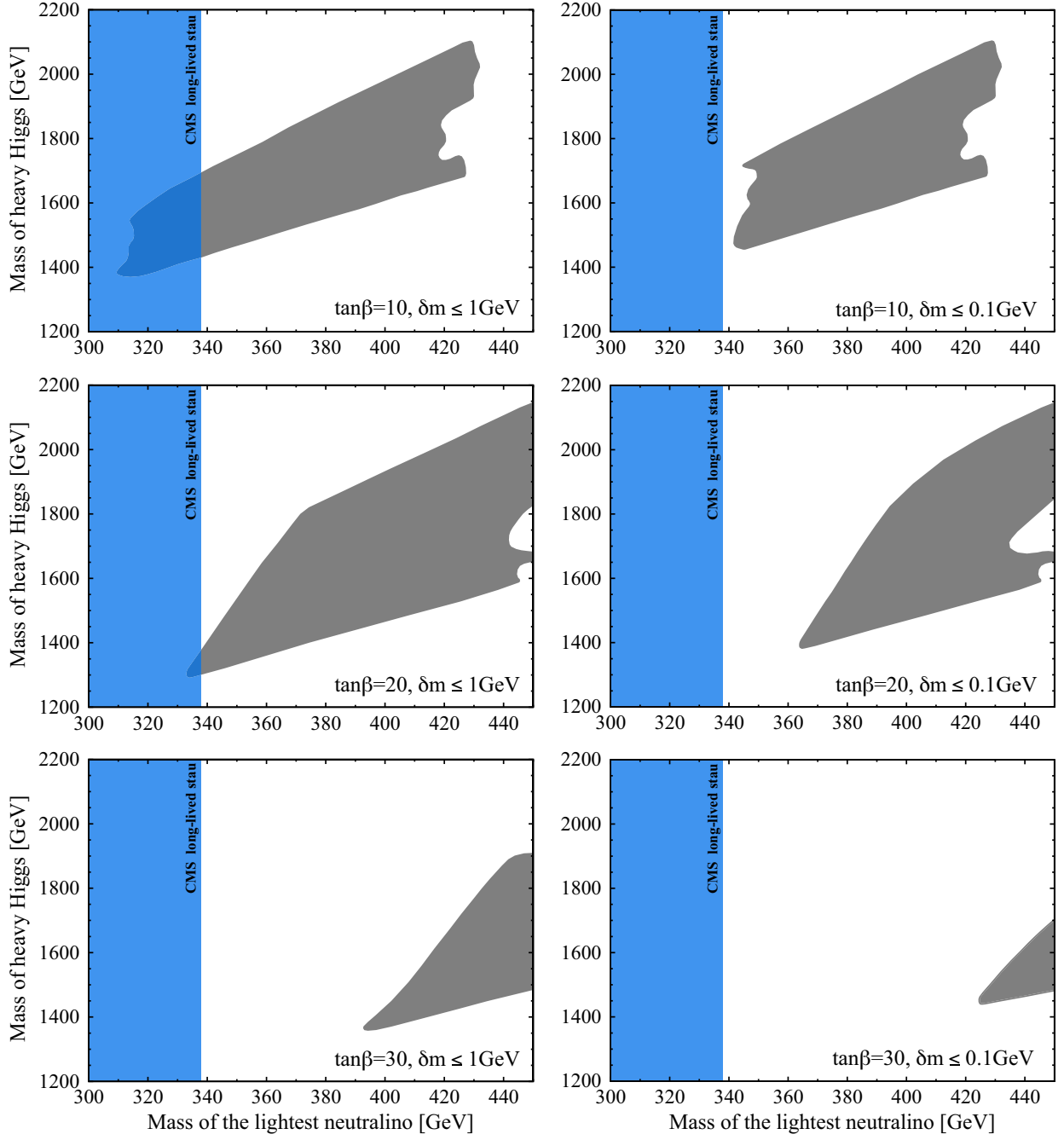


FIG. 9: Mass spectra of the heavy Higgs boson. The horizontal axis represents the mass of the LSP neutralino. We fix $\tan\beta$ to 10, 20 and 30 from top to bottom and $\delta m \leq 1$ and 0.1 GeV from left to right, respectively.

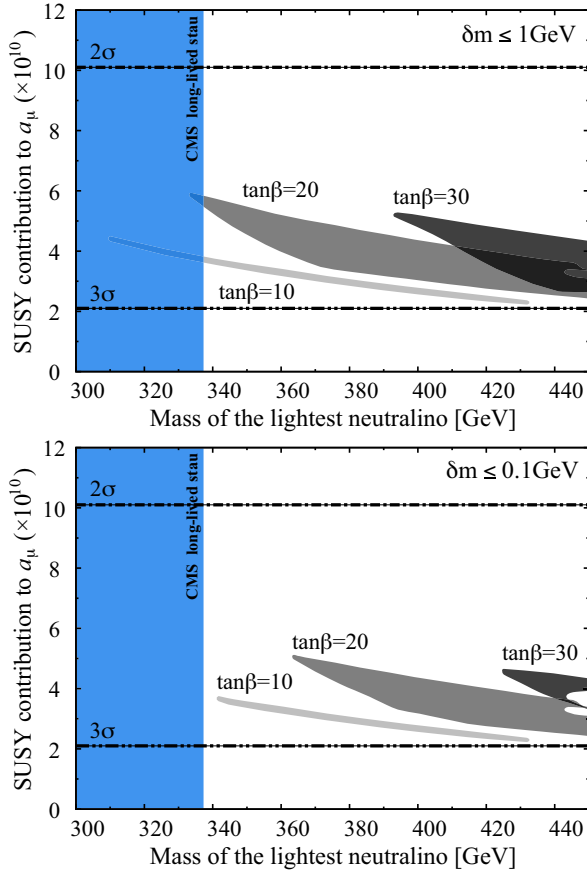


FIG. 10: Allowed values of δa_μ for neutralino mass. The upper and lower figures show the results corresponding to the cases of $\delta m \leq 1$ GeV and $\delta m \leq 0.1$ GeV, respectively.

B. Muon $g - 2$

We show the muon anomalous magnetic moment, $(g - 2)_\mu$, in the allowed region. The latest results on $(g - 2)_\mu$ have reported that there is a 3.3σ deviation between the SM prediction and the experimental data [78, 79]:

$$\delta a_\mu = a_\mu^{\text{exp}} - a_\mu^{\text{SM}} = (26.1 \pm 8.0) \times 10^{-10}, \quad (24)$$

where $a_\mu \equiv (g - 2)_\mu/2$.

For a fixed $\tan \beta$, lighter SUSY particles yield larger contributions. The masses are light as m_0 and $M_{1/2}$ are small. The small m_0 is, however, excluded by the constraint on the Higgs boson mass as shown in III B. The sizable contributions to δa_μ are obtained in the regions of small $M_{1/2}$. When we take into account $\delta m \leq 1$ and 0.1 GeV, the dominant SUSY contributions come from the smuon-bino like neutralino loop and the muon sneutrino-charged higgsino loop. Since we took $\mu > 0$, both contributions are positive. In Fig. 10, the SUSY contributions in the allowed region are shown for $\delta m \leq 1$ and 0.1 GeV in the top and the bottom panel, respectively. In the panels, $\tan \beta$ is taken to be 10, 20, and 30.

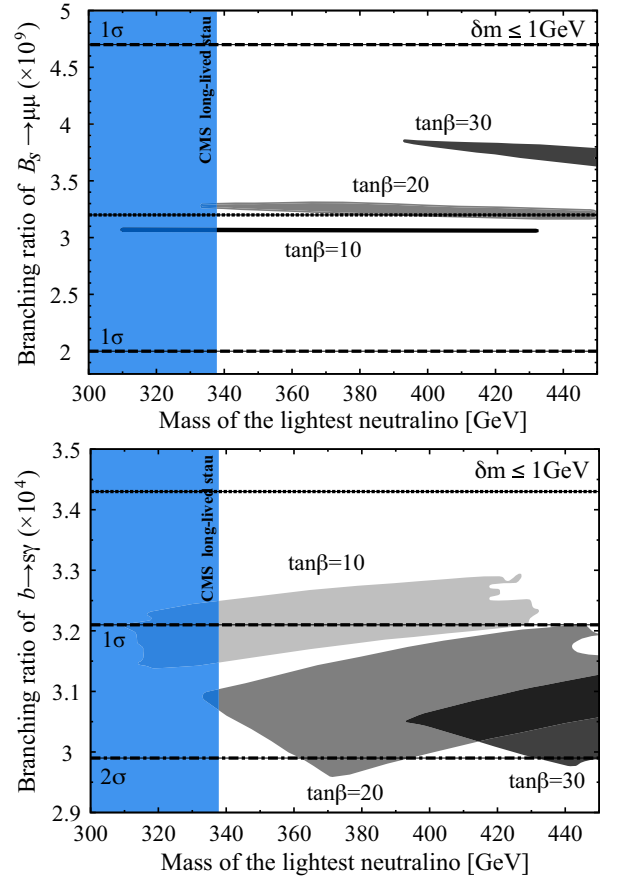


FIG. 11: Branching ratios of the decay processes of $B_s \rightarrow \mu^+ \mu^-$ and $B \rightarrow X_s \gamma$. We fix $\tan \beta$ to 10, 20, and 30, and $\delta m \leq 1$ GeV. The experimental values are indicated with the horizontal dotted lines.

It should be noted that the muon anomalous magnetic moment is consistent with current measurements within 3σ levels in this scenario.

C. Rare decays of B mesons

We show that the branching ratios of $B_s \rightarrow \mu^+ \mu^-$ and $B \rightarrow X_s \gamma$ are consistent with the experimental results.

The first evidence for the decay $B_s \rightarrow \mu^+ \mu^-$ has been discovered by the LHCb collaboration [80], and the branching ratio has been measured as

$$\text{BR}(B_s \rightarrow \mu^+ \mu^-) = (3.2^{+1.5}_{-1.2}) \times 10^{-9}. \quad (25)$$

It is also reported by [81] that the other important rare decay $B \rightarrow X_s \gamma$ is strongly suppressed as

$$\text{BR}(B \rightarrow X_s \gamma) = (3.43 \pm 0.21 \pm 0.07) \times 10^{-4}. \quad (26)$$

Figure 11 shows the branching ratios of the two rare decays for $\delta m \leq 1$ GeV. The top panel is for $B_s \rightarrow \mu^+ \mu^-$ and the bottom is for $B \rightarrow X_s \gamma$. One can see that the

N	$f_{T_u}^{(N)}$	$f_{T_d}^{(N)}$	$f_{T_s}^{(N)}$
p	0.0153	0.0191	0.0447
n	0.011	0.0273	0.0447

TABLE I: The mass fraction of light quarks in a proton p and a neutron n [67, 82].

branching ratios are within the 3σ in our allowed region, and hence are consistent with the experiments.

D. Direct detection of neutralino dark matter

One of the promising approaches to the neutralino dark matter is its direct detection. The scenario we are discussing can be examined by the direct detection measurements combining other measurements for the Higgs boson and the neutralino LSP.

The spin-independent (SI) scatterings are given by the Higgs and squarks exchanges. The squark exchange contributions are suppressed by heavy masses of squarks $m_{\tilde{q}}^{-4}$, where $m_{\tilde{q}} \simeq 2\text{TeV}$ in the scenario (see Fig. 5), and hence the SI scattering is dominated by the Higgs exchange contributions. In order to examine the scenario, we have to analyze the dependence of the SI scatterings on the measurements for the Higgs boson and neutralinos. The SI scattering cross section of the neutralino and target nucleon (T) is given by [83],

$$\sigma_{\text{SI}} = \frac{4}{\pi} \left(\frac{m_{\tilde{\chi}_1^0} m_T}{m_{\tilde{\chi}_1^0} + m_T} \right)^2 (n_p f_p + n_n f_n)^2, \quad (27)$$

where m_T is the mass of the target nucleus. The Symbol n_p (n_n) is the number of proton (neutron) in the target nucleus, and the effective coupling of the neutralino to a proton f_p is given as

$$\begin{aligned} f_p &= \sum_q f_q \langle p | \bar{q} q | p \rangle \\ &= \sum_{q=u,d,s} \frac{f_q}{m_q} m_p f_{T_q}^{(p)} + \frac{2}{27} f_{T_G} \sum_{q=c,b,t} \frac{f_q}{m_q} m_p, \end{aligned} \quad (28)$$

where $f_{T_q}^{(p)} \equiv \langle p | m_q \bar{q} q | p \rangle / m_p$ is the mass fraction of light quarks in a proton (listed in Table I), and $f_{T_G} = 1 - \sum_{u,d,s} f_{T_q}^{(p)}$. For the neutron, f_n is derived with the same manner. The effective coupling of the neutralino to quarks f_q is calculated as follows,

$$f_q = m_q \frac{g_2^2}{4m_W} \left(\frac{C_{h\tilde{\chi}_1^0\tilde{\chi}_1^0} C_{hqq}}{m_h^2} + \frac{C_{H\tilde{\chi}_1^0\tilde{\chi}_1^0} C_{Hqq}}{m_H^2} \right). \quad (29)$$

Here C_{hqq} and C_{Hqq} are the Yukawa couplings of the lighter and the heavier Higgs bosons and quarks (details formulae are given in Ref. [83]). For the bino-like neutralino LSP ($M_1 \ll M_2, \mu$), the coupling of the neutralino

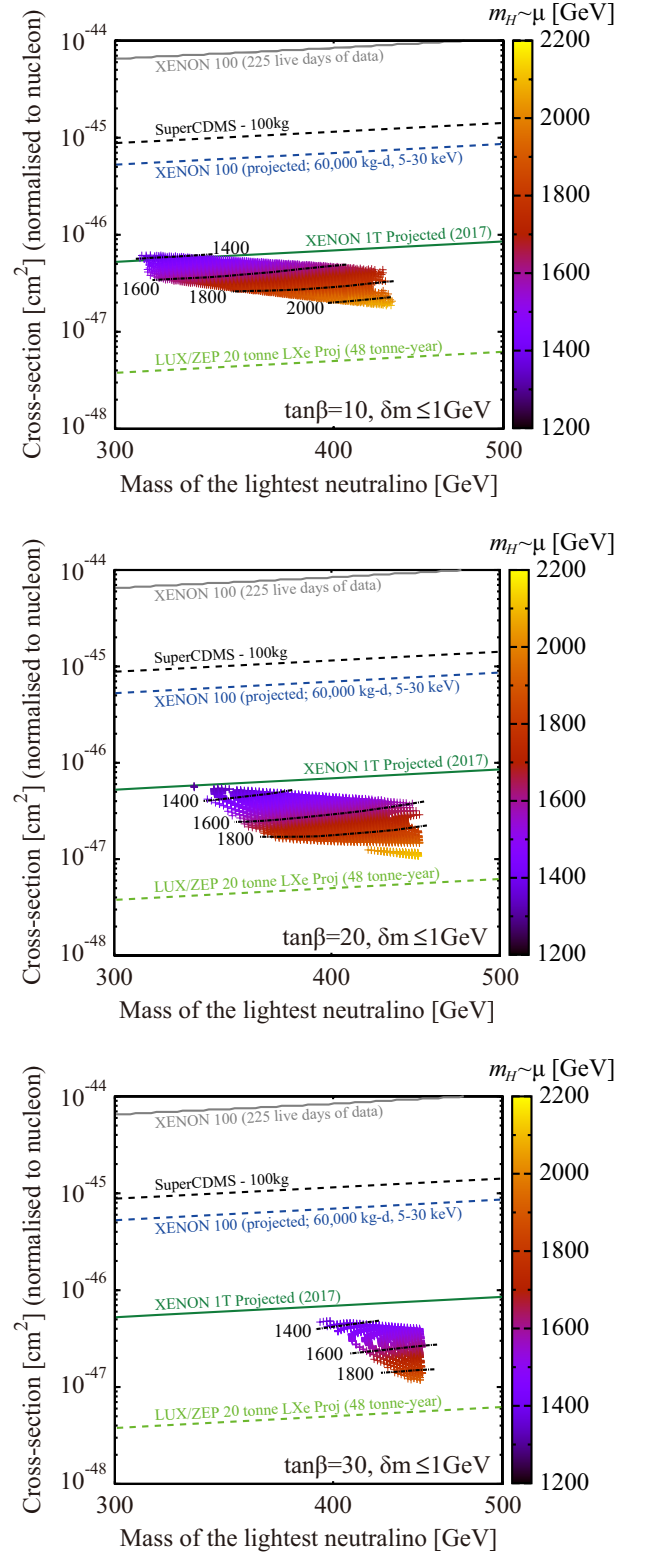


FIG. 12: Scatter plots of SI neutralino-nucleon cross section as a function of the mass of the neutralino dark matter. Each curves are shown for the current and future limit. A gradation of colors corresponds to the mass of the heavy Higgs boson.

and the Higgs bosons, $C_{h\tilde{\chi}_1^0\tilde{\chi}_1^0}$ and $C_{H\tilde{\chi}_1^0\tilde{\chi}_1^0}$, is perturbatively calculated as follows,

$$\begin{aligned} C_{h\tilde{\chi}_1^0\tilde{\chi}_1^0} &\simeq \frac{m_Z \sin \theta_W \tan \theta_W}{M_1^2 - \mu^2} [M_1 \sin \beta + \mu \cos \beta], \\ C_{H\tilde{\chi}_1^0\tilde{\chi}_1^0} &\simeq \frac{m_Z \sin \theta_W \tan \theta_W}{M_1^2 - \mu^2} \mu \sin \beta. \end{aligned} \quad (30)$$

In the scenario, the mass of the heavier CP-even Higgs boson is much larger than the mass of the lighter Higgs boson (see Fig. 9), and therefore the contribution from H exchange is negligible.

Figure 12 shows the Spin-Independent (SI) scattering cross section in the allowed region as a function of the mass of the neutralino dark matter for $\delta m \leq 1$ GeV, and $\tan \beta$ is taken to be 10, 20, and 30 from an upper panel to a lower one. Curves represent the current limit [84] and future limit [85, 86]. Colors correspond to the mass of the heavier CP-even Higgs boson.

In Fig. 12, we can see that the SI scattering cross section is smaller as $\tan \beta$ and/or the neutralino mass is larger. Such behavior can be easily understood by Eq.(30). We can also see from the contour lines that the lighter mass of the heavy Higgs boson leads larger SI cross sections for all $\tan \beta$. This is understood as follows. The mass of the heavy Higgs boson is determined by the condition of the radiative electroweak symmetry breaking in the scenario, and is almost equal to $m_H \simeq \mu$ (see the discussion in Subsec. IV A). As is given in Eq. (30), smaller μ makes the neutralino mixing to be larger value, and hence large couplings between the neutralino dark matter and the Higgs bosons are obtained. Thus a clear correlation of the mass of the heavy Higgs boson and the cross section is appeared.

In the end, one can see that future direct detection experiments will reach to the sensitivity to detect the neutralino dark matter in the scenario. The mass of the heavy Higgs boson can be estimated from the measurements of the cross section and the mass of the neutralino at the direct detection and the LHC experiments. Thus the interplay of both experiments will play important roles to examine our scenario.

V. DIRECT SEARCH AT THE LHC

We here estimate the number of events of the long-lived stau and the neutralino at the LHC with the center of mass energy 14TeV, and consider the feasibility of the verification of the scenario.

We choose five sets of the CMSSM parameters in the allowed region for $\tan \beta = 20$. The parameters of the sample points and the mass spectrum of the SUSY particles are shown in Table II. These points correspond to the mass of the neutralino, 350, 375, 400, 425, and 450GeV, respectively. We calculate the branching ratios and the pair production cross sections of SUSY particles with CalcHEP 3.4 [87]. The branching ratios are shown in Tables III and IV. The first column is the parent particles

and the second one is the final states. The production cross sections of SUSY particles are shown in Tables V and VI. The first column $\sigma(a, b)$ is the production cross sections of particles a and b from p - p collision with the center of mass energy 14TeV. The last row of Table VI, $\sigma(\text{all SUSY})$, is the sum of the production cross sections of SUSY particles.

Using the numbers given in the Tables, we calculate the number of the stau from SUSY cascade decays and direct productions. The branching fraction of the cascade decays of a SUSY particle $\tilde{\psi}$ to the stau is denoted as $\text{BR}(\tilde{\psi} \rightarrow \tilde{\tau}_1)$. The symbol $\sigma(\tilde{\psi})$ represents the sum of the cross sections of the SUSY particles. Then the effective total production cross section of the stau is

$$\sigma(\tilde{\tau}_1^{(*)}) = \sum_{\tilde{\psi}}^{\text{all SUSY}} \sigma(\tilde{\psi}) \times \text{BR}(\tilde{\psi} \rightarrow \tilde{\tau}_1^{(*)}). \quad (31)$$

Since the long-lived staus penetrate the LHC detectors, the number of missing energy is calculated as follows,

$$N(\tilde{\chi}_1^0) = \{\sigma(\text{all SUSY}) - \sigma(\tilde{\tau}_1) - \sigma(\tilde{\tau}_1^{*})\} \times \mathcal{L}_{\text{int}}, \quad (32)$$

where \mathcal{L}_{int} is the integrated luminosity. Assuming an integrated luminosity is $\mathcal{L}_{\text{int}} = 100\text{fb}^{-1}$, the expected number of the stau and the neutralino is 3900 and 3700 for $m_{\tilde{\tau}_1} = 350\text{GeV}$, and 710 and 980 for $m_{\tilde{\tau}_1} = 450\text{GeV}$ (see Table VII). These numbers will be enough to examine the scenario⁴.

In Table VI, one can see that the production cross sections of stops are comparable to those of gluinos and light squarks. Those are obtained as 4.40 fb for $m_{\tilde{\tau}_1} = 350\text{GeV}$ and 2.66fb for $m_{\tilde{\tau}_1} = 450\text{GeV}$. It is important to emphasize here that such production cross sections of stops are the results of our constraint that leads to relatively heavy SUSY spectrum. Therefore early discovery of the stop at the 14 TeV run is one of the predictions in the scenario.

⁴ The efficiency to identify the stau and the neutralino with 350 and 450GeV is about $\mathcal{O}(10)\%$ in [76]. Thus it is possible to examine our scenario with $\mathcal{L}_{\text{int}} = 100\text{fb}^{-1}$. Detailed simulation is beyond the scope of this paper and is left for our future work.

Input Parameters	Point 1 [GeV]	Point 2 [GeV]	Point 3 [GeV]	Point 4 [GeV]	Point 5 [GeV]
$M_{1/2}$	818.6	878.0	932.8	986.0	1038.0
m_0	452.0	517.7	557.7	601.7	639.7
A_0	-2264.7	-2683.6	-2918.4	-3177.9	-3397.0
Particle					
h	123.8	124.4	124.6	124.8	124.9
H	1494.6	1659.5	1775.7	1894.0	2002.0
A	1495.1	1660.3	1776.5	1895.1	2003.3
H^\pm	1497.0	1662.0	1778.1	1896.5	2004.6
\tilde{g}	1822.4	1945.4	2057.8	2166.7	2272.6
$\tilde{\chi}_1^\pm$	665.6	716.3	762.4	807.4	851.2
$\tilde{\chi}_2^\pm$	1470.6	1638.9	1753.5	1873.7	1981.4
$\tilde{\chi}_1^0$	349.3	376.3	400.9	425.0	448.5
$\tilde{\chi}_2^0$	665.3	716.1	762.4	807.4	851.2
$\tilde{\chi}_3^0$	1466.8	1635.3	1750.1	1870.5	1978.4
$\tilde{\chi}_4^0$	1469.7	1638.4	1753.1	1873.3	1981.0
\tilde{e}_L	709.6	781.6	834.9	890.0	940.6
\tilde{e}_R	547.5	614.2	658.7	706.2	748.6
$\tilde{\nu}_e$	749.2	777.4	830.9	886.2	937.0
$\tilde{\tau}_1$	350.3	377.0	401.0	425.6	449.1
$\tilde{\tau}_2$	656.0	713.7	759.3	805.9	849.4
$\tilde{\nu}_\tau$	642.7	701.2	747.4	794.6	838.7
\tilde{u}_L	1710.9	1834.4	1942.2	2048.0	2149.7
\tilde{u}_R	1646.6	1765.6	1869.0	1970.6	2068.0
\tilde{d}_L	1712.6	1835.9	1943.7	2049.4	2151.0
\tilde{d}_R	1639.9	1758.3	1861.1	1962.1	2059.0
\tilde{t}_1	945.8	936.5	968.6	987.7	1016.3
\tilde{t}_2	1432.8	1497.5	1573.1	1641.3	1710.8
\tilde{b}_1	1384.6	1452.8	1528.4	1598.2	1669.3
\tilde{b}_2	1561.6	1665.8	1760.5	1852.6	1942.0

TABLE II: Input parameters and the mass spectrum of sample points. The value of $\tan\beta$ is fixed to 20 and $\text{sign}(\mu) > 0$. We choose these parameters as the $m_{\tilde{\chi}_1^0}$ is fixed to 350, 375, 400, 425, and 450 GeV, respectively.

Particle	Final States	Point1 [%]	Point2 [%]	Point3 [%]	Point4 [%]	Point5 [%]
\tilde{g}	\bar{t}, \tilde{t}_1	21.4	22.6	22.9	23.3	23.6
	t, \tilde{t}_1^*	21.4	22.6	22.9	23.3	23.6
	\bar{b}, \tilde{b}_1	8.3	8.4	8.4	8.5	8.5
	b, \tilde{b}_1^*	8.3	8.4	8.4	8.5	8.5
	\bar{t}, \tilde{t}_2	7.9	8.2	8.3	8.3	8.4
	t, \tilde{t}_2^*	7.9	8.2	8.3	8.3	8.4
	\bar{b}, \tilde{b}_2	3.3	3.1	3.0	3.0	2.9
	b, \tilde{b}_2^*	3.3	3.1	3.0	3.0	2.9
\tilde{u}_L	$d, \tilde{\chi}_1^+$	65.8	65.8	65.8	65.8	65.7
	$u, \tilde{\chi}_2^0$	32.8	32.9	32.9	32.9	32.9
	$u, \tilde{\chi}_1^0$	1.4	1.4	1.4	1.4	1.4
\tilde{d}_L	$u, \tilde{\chi}_1^-$	65.6	65.6	65.7	65.7	65.7
	$d, \tilde{\chi}_2^0$	32.9	32.9	32.9	32.9	32.9
	$d, \tilde{\chi}_1^0$	1.5	1.5	1.5	1.5	1.5
\tilde{t}_1	$t, \tilde{\chi}_1^0$	78.4	86.3	89.4	92.7	94.8
	$b, \tilde{\chi}_1^+$	15.8	10.5	8.3	6.0	4.6
	$t, \tilde{\chi}_2^0$	5.9	3.2	2.4	1.3	0.6
\tilde{t}_2	Z, \tilde{t}_1	41.7	43.5	43.7	44.1	44.3
	h, \tilde{t}_1	29.1	32.0	33.2	34.4	35.3
	$b, \tilde{\chi}_1^+$	19.1	16.0	15.1	14.0	13.4
	$t, \tilde{\chi}_2^0$	9.1	7.7	7.2	6.7	6.4
\tilde{b}_1	W^-, \tilde{t}_1	69.9	83.7	76.9	78.7	79.8
	$t, \tilde{\chi}_1^-$	19.3	15.9	14.9	13.7	13.0
	$b, \tilde{\chi}_2^0$	10.2	8.4	7.8	7.9	6.8
\tilde{b}_2	W^-, \tilde{t}_1	44.0	39.7	36.5	33.4	30.9
	$h, \tilde{\chi}_1^0$	31.6	30.2	30.2	29.8	29.7
	h, \tilde{b}_1	9.4	12.6	13.8	15.0	15.8
	Z, \tilde{b}_1	5.7	7.7	8.5	9.4	9.9
	W^-, \tilde{t}_2	3.3	6.6	8.3	10.2	11.7
	$t, \tilde{\chi}_1^-$	2.9	2.1	1.8	1.5	1.3
	$b, \tilde{\chi}_2^0$	1.5	1.1	0.9	0.8	0.7
$\tilde{\nu}_\tau$	$W^+, \tilde{\tau}_1$	81.8	83.0	83.4	83.8	84.0
	$\nu_\tau, \tilde{\chi}_1^0$	18.2	17.0	16.6	16.2	16.0
$\tilde{\tau}_2$	$Z, \tilde{\tau}_1$	41.3	41.8	41.9	42.0	42.0
	$h, \tilde{\tau}_1$	39.0	39.9	40.5	40.9	41.2
	$\tau, \tilde{\chi}_1^0$	19.7	18.3	17.7	14.2	16.8
$\tilde{\chi}_2^0$	$\bar{\tau}, \tilde{\tau}_1$	40.1	45.0	45.0	46.1	46.2
	$\tau, \tilde{\tau}_1^*$	40.1	45.0	45.0	46.1	46.2
	$\bar{\nu}_\tau, \tilde{\nu}_\tau$	7.3	3.6	3.6	2.6	2.5
	$\nu_\tau, \tilde{\nu}^*$	7.3	3.6	3.6	2.6	2.5
	$h, \tilde{\chi}_1^0$	2.5	2.5	2.5	2.5	2.4

TABLE III: Branching ratios of the SUSY particles on the sample points.

Particle	Final States	Point1 [%]	Point2 [%]	Point3 [%]	Point4 [%]	Point5 [%]
$\tilde{\chi}_3^0$	\bar{t}, \tilde{t}_1	22.6	26.7	26.7	26.9	27.0
	t, \tilde{t}_1^*	22.6	26.7	26.7	26.9	27.0
	$W^-, \tilde{\chi}_1^+$	15.0	12.6	11.6	10.7	10.3
	$W^+, \tilde{\chi}_1^-$	15.0	12.6	11.6	10.7	10.3
	$Z, \tilde{\chi}_2^0$	13.2	11.0	10.1	9.3	8.9
	$Z, \tilde{\chi}_1^0$	4.0	3.3	3.0	2.8	2.7
	$h, \tilde{\chi}_2^0$	1.6	1.4	1.3	1.3	1.2
	\bar{t}, \tilde{t}_2	—	—	1.8	3.1	3.7
	t, \tilde{t}_2^*	—	—	1.8	3.1	3.7
$\tilde{\chi}_4^0$	\bar{t}, \tilde{t}_1	27.0	29.8	29.9	30.0	29.9
	t, \tilde{t}_1^*	27.0	29.8	29.9	30.0	29.9
	$W^-, \tilde{\chi}_1^+$	12.3	10.7	10.3	9.8	9.5
	$W^+, \tilde{\chi}_1^-$	12.3	10.7	10.3	9.8	9.5
	$h, \tilde{\chi}_2^0$	11.4	9.9	9.6	9.1	8.9
	$h, \tilde{\chi}_1^0$	3.1	2.6	2.5	2.4	2.3
	$Z, \tilde{\chi}_2^0$	1.3	1.2	1.2	1.1	1.1
$\tilde{\chi}_1^+$	$\nu_\tau, \tilde{\tau}_1^*$	79.3	89.1	89.2	91.3	91.5
	$\bar{\tau}, \tilde{\nu}_\tau$	15.0	7.5	7.3	5.4	5.2
	$W^+, \tilde{\chi}_1^0$	3.1	3.2	3.1	3.2	3.2
$\tilde{\chi}_2^+$	\bar{b}, \tilde{t}_1	48.4	53.0	53.3	53.9	54.1
	$h, \tilde{\chi}_1^+$	14.2	11.9	11.3	10.6	10.3
	$Z, \tilde{\chi}_1^+$	13.8	11.5	10.9	10.2	9.9
	$W^+, \tilde{\chi}_2^0$	14.0	11.7	11.1	10.4	10.0
	$W^+, \tilde{\chi}_1^0$	4.7	3.9	3.7	3.5	3.4
	t, \tilde{b}_1^*	4.8	3.4	5.1	6.8	7.8
	$\nu_\tau, \tilde{\tau}_1^*$	2.1	1.8	1.8	1.7	1.6
	$\bar{\tau}, \tilde{\nu}_\tau$	1.9	1.6	1.5	1.4	1.4
H	b, \bar{b}	63.3	61.1	60.4	59.6	59.2
	$\tau, \bar{\tau}$	11.6	11.4	11.4	11.3	11.3
	$\tilde{\tau}_1, \tilde{\tau}_2^*$	10.0	11.3	11.7	12.2	12.6
	$\tilde{\tau}_1^*, \tilde{\tau}_2$	10.0	11.3	11.7	12.2	12.6
	$\tilde{\tau}_1^*, \tilde{\tau}_1$	1.9	1.8	1.7	1.6	1.4
	t, \bar{t}	1.6	1.6	1.6	1.6	1.6
A	b, \bar{b}	62.4	60.8	60.2	59.5	59.1
	$\tau, \bar{\tau}$	11.6	11.4	11.3	11.3	11.3
	$\tilde{\tau}_1, \tilde{\tau}_2^*$	11.5	12.7	13.1	13.5	13.7
	$\tilde{\tau}_1^*, \tilde{\tau}_2$	11.5	12.7	13.1	13.5	13.7
	t, \bar{t}	1.6	1.5	1.5	1.5	1.5
H^+	\bar{b}, t	62.9	63.9	64.8	65.2	66.2
	$\tilde{\tau}_1, \tilde{\nu}_\tau$	25.9	24.9	23.9	23.4	22.2
	$\bar{\tau}, \nu_\tau$	10.3	10.5	10.6	10.8	11.0

TABLE IV: Branching ratios of the SUSY particles on the sample points.

Cross Section	Point1 [fb]	Point2 [fb]	Point3 [fb]	Point4 [fb]	Point5 [fb]
$\sigma(\tilde{u}_L, \tilde{u}_L)$	2.915	1.873	1.277	0.879	0.614
$\sigma(\tilde{u}_L, \tilde{u}_R)$	1.672	1.024	0.668	0.441	0.296
$\sigma(\tilde{u}_R, \tilde{u}_R)$	2.970	1.926	1.327	0.923	0.652
$\sigma(\tilde{d}_L, \tilde{d}_L)$	0.377	0.225	0.144	0.095	0.061
$\sigma(\tilde{d}_L, \tilde{d}_R)$	0.194	0.110	0.068	0.042	0.026
$\sigma(\tilde{d}_R, \tilde{d}_R)$	0.381	0.230	0.149	0.098	0.065
$\sigma(\tilde{u}_L, \tilde{d}_L)$	3.243	2.016	1.335	0.894	0.608
$\sigma(\tilde{u}_L, \tilde{d}_R)$	0.557	0.329	0.208	0.133	0.087
$\sigma(\tilde{u}_R, \tilde{d}_L)$	0.551	0.325	0.205	0.131	0.086
$\sigma(\tilde{u}_R, \tilde{d}_R)$	2.680	1.680	1.124	0.759	0.522
$\sigma(\tilde{g}, \tilde{u}_L)$	2.735	1.506	0.899	0.537	0.330
$\sigma(\tilde{g}, \tilde{u}_R)$	3.156	1.750	1.041	0.633	0.391
$\sigma(\tilde{g}, \tilde{d}_L)$	0.826	0.440	0.252	0.148	0.088
$\sigma(\tilde{g}, \tilde{d}_R)$	0.981	0.527	0.305	0.180	0.109
$\sigma(\tilde{g}, \tilde{g})$	0.440	0.219	0.118	0.065	0.037
$\sigma(\tilde{u}_L, \tilde{u}_L^*)$	0.059	0.032	0.019	0.012	0.006
$\sigma(\tilde{u}_L, \tilde{u}_R^*)$	0.220	0.126	0.078	0.049	0.031
$\sigma(\tilde{u}_R, \tilde{u}_L^*)$	0.220	0.126	0.078	0.049	0.031
$\sigma(\tilde{u}_R, \tilde{u}_R^*)$	0.084	0.047	0.027	0.016	0.011
$\sigma(\tilde{d}_L, \tilde{d}_L^*)$	0.037	0.019	0.011	0.006	0.003
$\sigma(\tilde{d}_L, \tilde{d}_R^*)$	0.080	0.042	0.024	0.014	0.008
$\sigma(\tilde{d}_R, \tilde{d}_L^*)$	0.080	0.042	0.024	0.014	0.008
$\sigma(\tilde{d}_R, \tilde{d}_R^*)$	0.052	0.027	0.016	0.008	0.003
$\sigma(\tilde{u}_L, \tilde{d}_R^*)$	0.254	0.139	0.083	0.050	0.030
$\sigma(\tilde{u}_R, \tilde{d}_L^*)$	0.249	0.136	0.081	0.048	0.029
$\sigma(\tilde{u}_L, \tilde{d}_L^*)$	0.035	0.018	0.010	0.005	0.003
$\sigma(\tilde{u}_R, \tilde{d}_R^*)$	0.056	0.029	0.017	0.009	0.006
$\sigma(\tilde{d}_L, \tilde{u}_L^*)$	0.010	0.005	0.003	0.002	0.001
$\sigma(\tilde{d}_R, \tilde{u}_L^*)$	0.069	0.038	0.023	0.014	0.009
$\sigma(\tilde{d}_L, \tilde{u}_R^*)$	0.069	0.037	0.022	0.014	0.008
$\sigma(\tilde{d}_R, \tilde{u}_R^*)$	0.015	0.008	0.005	0.003	0.002
$\sigma(\tilde{g}, \tilde{u}_L^*)$	0.051	0.025	0.014	0.008	0.004
$\sigma(\tilde{g}, \tilde{u}_R^*)$	0.061	0.030	0.017	0.009	0.005
$\sigma(\tilde{g}, \tilde{d}_L^*)$	0.045	0.021	0.011	0.006	0.003
$\sigma(\tilde{g}, \tilde{d}_R^*)$	0.056	0.027	0.014	0.007	0.004

TABLE V: Cross sections of SUSY particles on the sample points. We assume the energy in the center of mass system as 14 TeV at LHC experiment.

Cross Section	Point1 [fb]	Point2 [fb]	Point3 [fb]	Point4 [fb]	Point5 [fb]
$\sigma(\tilde{t}_1, \tilde{t}_1^*)$	4.399	4.704	3.662	3.245	2.655
$\sigma(\tilde{t}_2, \tilde{t}_2^*)$	0.180	0.129	0.085	0.058	0.039
$\sigma(\tilde{b}_1, \tilde{b}_1^*)$	0.252	0.169	0.108	0.074	0.050
$\sigma(\tilde{b}_2, \tilde{b}_2^*)$	0.089	0.050	0.030	0.018	0.011
$\sigma(\tilde{\chi}_2^0, \tilde{\chi}_2^0)$	0.051	0.035	0.024	0.018	0.013
$\sigma(\tilde{\chi}_1^0, \tilde{\chi}_1^0)$	0.103	0.037	0.028	0.022	0.018
$\sigma(\tilde{\chi}_2^0, \tilde{g})$	0.101	0.062	0.040	0.026	0.017
$\sigma(\tilde{\chi}_1^0, \tilde{g})$	0.114	0.073	0.049	0.034	0.023
$\sigma(\tilde{\chi}_1^+, \tilde{\chi}_1^-)$	1.229	0.861	0.629	0.470	0.355
$\sigma(\tilde{\chi}_1^+, \tilde{\chi}_2^0)$	3.514	2.499	1.858	1.404	1.075
$\sigma(\tilde{\chi}_1^-, \tilde{\chi}_2^0)$	1.232	0.852	0.616	0.455	0.341
$\sigma(\tilde{\chi}_1^+, \tilde{\chi}_1^0)$	0.023	0.017	0.012	0.005	0.003
$\sigma(\tilde{\chi}_1^-, \tilde{\chi}_1^0)$	0.008	0.005	0.004	0.003	0.002
$\sigma(\tilde{\chi}_1^+, \tilde{g})$	0.344	0.209	0.134	0.087	0.058
$\sigma(\tilde{\chi}_1^-, \tilde{g})$	0.094	0.057	0.037	0.024	0.016
$\sigma(\tilde{\tau}_1, \tilde{\tau}_1^*)$	0.422	0.313	0.241	0.188	0.149
$\sigma(\text{all SUSY})$	37.730	25.268	17.277	12.445	8.456

TABLE VI: Cross sections of SUSY particles on the sample points. We assume the energy in the center of mass system as 14 TeV at LHC experiment.

Cross Section \times Branching Ratio	Point1 [fb]	Point2 [fb]	Point3 [fb]	Point4 [fb]	Point5 [fb]
$\sigma(\tilde{g}) \times \text{BR}(\tilde{g} \rightarrow \tilde{\tau}_1)$	1.105	0.452	0.224	0.108	0.060
$\sigma(\tilde{g}) \times \text{BR}(\tilde{g} \rightarrow \tilde{\tau}_1^*)$	1.105	0.452	0.224	0.108	0.060
$\sigma(\tilde{u}_L) \times \text{BR}(\tilde{u}_L \rightarrow \tilde{\tau}_1)$	3.391	1.779	1.161	0.733	0.284
$\sigma(\tilde{u}_L) \times \text{BR}(\tilde{u}_L \rightarrow \tilde{\tau}_1^*)$	11.021	7.023	4.600	3.066	1.195
$\sigma(\tilde{d}_L) \times \text{BR}(\tilde{d}_L \rightarrow \tilde{\tau}_1)$	4.203	2.618	1.682	1.103	0.730
$\sigma(\tilde{d}_L) \times \text{BR}(\tilde{d}_L \rightarrow \tilde{\tau}_1^*)$	1.297	0.665	0.425	0.264	0.174
$\sigma(\tilde{t}_1) \times \text{BR}(\tilde{t}_1 \rightarrow \tilde{\tau}_1)$	0.204	0.103	0.060	0.029	0.013
$\sigma(\tilde{t}_1) \times \text{BR}(\tilde{t}_1 \rightarrow \tilde{\tau}_1^*)$	0.755	0.544	0.330	0.207	0.125
$\sigma(\tilde{t}_2) \times \text{BR}(\tilde{t}_2 \rightarrow \tilde{\tau}_1)$	0.019	0.008	0.005	0.003	0.002
$\sigma(\tilde{t}_2) \times \text{BR}(\tilde{t}_2 \rightarrow \tilde{\tau}_1^*)$	0.064	0.036	0.021	0.013	0.008
$\sigma(\tilde{b}_1) \times \text{BR}(\tilde{b}_1 \rightarrow \tilde{\tau}_1)$	0.053	0.029	0.017	0.010	0.006
$\sigma(\tilde{b}_1) \times \text{BR}(\tilde{b}_1 \rightarrow \tilde{\tau}_1^*)$	0.036	0.018	0.008	0.004	0.002
$\sigma(\tilde{b}_2) \times \text{BR}(\tilde{b}_2 \rightarrow \tilde{\tau}_1)$	0.008	0.004	0.002	0.001	0.001
$\sigma(\tilde{b}_2) \times \text{BR}(\tilde{b}_2 \rightarrow \tilde{\tau}_1^*)$	0.010	0.005	0.002	0.001	0.001
$\sigma(\tilde{u}_L^*) \times \text{BR}(\tilde{u}_L^* \rightarrow \tilde{\tau}_1)$	0.161	0.092	0.056	0.035	0.021
$\sigma(\tilde{u}_L^*) \times \text{BR}(\tilde{u}_L^* \rightarrow \tilde{\tau}_1^*)$	0.099	0.047	0.028	0.017	0.010
$\sigma(\tilde{d}_L^*) \times \text{BR}(\tilde{d}_L^* \rightarrow \tilde{\tau}_1)$	0.107	0.049	0.028	0.015	0.009
$\sigma(\tilde{d}_L^*) \times \text{BR}(\tilde{d}_L^* \rightarrow \tilde{\tau}_1^*)$	0.348	0.191	0.111	0.065	0.037
$\sigma(\tilde{t}_1^*) \times \text{BR}(\tilde{t}_1^* \rightarrow \tilde{\tau}_1)$	0.755	0.544	0.330	0.207	0.125
$\sigma(\tilde{t}_1^*) \times \text{BR}(\tilde{t}_1^* \rightarrow \tilde{\tau}_1^*)$	0.204	0.103	0.060	0.029	0.013
$\sigma(\tilde{t}_2^*) \times \text{BR}(\tilde{t}_2^* \rightarrow \tilde{\tau}_1)$	0.064	0.036	0.021	0.013	0.008
$\sigma(\tilde{t}_2^*) \times \text{BR}(\tilde{t}_2^* \rightarrow \tilde{\tau}_1^*)$	0.019	0.008	0.005	0.003	0.002
$\sigma(\tilde{b}_1^*) \times \text{BR}(\tilde{b}_1^* \rightarrow \tilde{\tau}_1)$	0.036	0.018	0.008	0.004	0.002
$\sigma(\tilde{b}_1^*) \times \text{BR}(\tilde{b}_1^* \rightarrow \tilde{\tau}_1^*)$	0.053	0.029	0.017	0.010	0.006
$\sigma(\tilde{b}_2^*) \times \text{BR}(\tilde{b}_2^* \rightarrow \tilde{\tau}_1)$	0.010	0.005	0.002	0.001	0.001
$\sigma(\tilde{b}_2^*) \times \text{BR}(\tilde{b}_2^* \rightarrow \tilde{\tau}_1^*)$	0.008	0.004	0.002	0.001	0.001
$\sigma(\tilde{\chi}_2^0) \times \text{BR}(\tilde{\chi}_2^0 \rightarrow \tilde{\tau}_1)$	2.281	1.672	1.229	0.928	0.705
$\sigma(\tilde{\chi}_2^0) \times \text{BR}(\tilde{\chi}_2^0 \rightarrow \tilde{\tau}_1^*)$	2.281	1.672	1.229	0.928	0.705
$\sigma(\tilde{\chi}_1^+) \times \text{BR}(\tilde{\chi}_1^+ \rightarrow \tilde{\tau}_1)$	0.627	0.223	0.162	0.090	0.065
$\sigma(\tilde{\chi}_1^+) \times \text{BR}(\tilde{\chi}_1^+ \rightarrow \tilde{\tau}_1^*)$	4.679	3.418	2.510	1.885	1.430
$\sigma(\tilde{\chi}_1^-) \times \text{BR}(\tilde{\chi}_1^- \rightarrow \tilde{\tau}_1)$	2.347	1.692	1.226	0.913	0.685
$\sigma(\tilde{\chi}_1^-) \times \text{BR}(\tilde{\chi}_1^- \rightarrow \tilde{\tau}_1^*)$	0.314	0.110	0.079	0.043	0.031
$\sigma(p \rightarrow \tilde{\tau}_1)$	0.422	0.313	0.241	0.188	0.149
$\sigma(p \rightarrow \tilde{\tau}_1^*)$	0.422	0.313	0.241	0.188	0.149
Total : $\sigma(\tilde{\tau}_1)$	15.954	9.728	7.739	4.415	2.885
Total : $\sigma(\tilde{\tau}_1^*)$	22.715	16.310	9.893	6.831	3.948
Number of produced $\tilde{\tau}_1^{(*)}$					
$N(\tilde{\tau}_1)$	1595	972	773	441	288
$N(\tilde{\tau}_1^*)$	2271	1631	989	683	394
Number of produced $\tilde{\chi}_1^0$					
$N(\tilde{\chi}_1^0)$	3679	2449	1692	1364	1007

TABLE VII: Summary of the cross sections and the branching ratios, and number of the produced tau and neutralino. We assume the energy in the center of mass system as 14 TeV at LHC experiment. In the estimation of number of produced tau and neutralino, we assume the luminosity as 100 fb^{-1} .

VI. SUMMARY

We have studied the scenario of the CMSSM in which the so-called lithium-7 problem can be solved via internal conversion processes with long-lived staus. For the abundance of lithium-7 to be reduced to the observed one, we imposed the following conditions, that (i) the mass difference of the stau NLSP and the neutralino LSP is smaller than 0.1 (1)GeV, and (ii) the yield value of the stau NLSP is larger than 10^{-13} . The first condition that guarantees enough long lifetime of the stau constrains the stau mass for a fixed neutralino mass, hence the scalar soft mass m_0 and the trilinear coupling A_0 , while the second one that guarantees the sufficient reduction of the lithium-7 constrains the upper bound on the neutralino mass or the gaugino soft mass $M_{1/2}$. We analyzed the parameter space as well as the SUSY spectrum of the CMSSM by taking the recent results on the Higgs mass, SUSY searches and the dark matter abundance into account.

In Sec. III, we have shown the allowed region on the A_0 - m_0 and m_0 - $M_{1/2}$ plane for $\delta m \leq 0.1$ and 1GeV varying $\tan\beta = 10, 20$ and 30, respectively. We found a linear relation between A_0 and m_0 in all cases as given in Eq.(12). The relation originates from the tightly degenerate mass of the stau and the relic abundance of the neutralino. It was also found that the allowed region on A_0 - m_0 plane shifts to higher scale as $\tan\beta$ increases. Thus the SUSY spectrum is heavier for large $\tan\beta$. On the other hand, as seen in Fig.3, $M_{1/2}$ is constrained between 750(950) and 1050GeV for $\tan\beta = 10(30)$. The upper bound comes from the yield value of the stau while the lower one from the small mass difference and the dark matter abundance. Thus, the conditions required to solve the lithium-7 problem play an important role to determine the allowed region of the CMSSM parameters. Notably, these results naturally lead to heavy SUSY spectrum. The bounds on $M_{1/2}$ lead to the stau mass between 310(400) and 450GeV. Such heavy staus evade the present bound from direct searches at LHC.

In Figs.5-9, we have shown the SUSY spectrum and the heavier Higgs mass in the allowed region. One can see that the whole spectrum is relatively heavy so that it is consistent with the null results of the SUSY searches at the LHC experiment. Among the spectrum, one of the important predictions is the masses of the gluino and the 1st/2nd generation squarks. In Fig.5, it was shown that the masses are clearly correlated with the neutralino

mass. This is the direct consequences from the linear relation of A_0 and m_0 . Thus in our scenario, once one of them is determined, the others can be predicted. It is important to emphasize here that the masses of gluino and squarks are constrained between 1.6(1.8) and 2.3TeV for $\tan\beta = 10(30)$. These gluino and squark masses are out of reach at 8 TeV LHC run but really in reach of 14TeV LHC run. The expected numbers of the long-lived staus (nearly degenerate neutralino) to 100fb^{-1} are about 3900 (3700) for the light neutralino mass and 710 (980) for the heavy one, respectively. With these numbers, the long-lived stau and the nearly degenerate neutralino will be identified easily. Thus our scenario explains why SUSY has not been found yet, and at the same time predicts the early discovery of SUSY in the coming few years. The other important prediction is the stop mass. The stops are also relatively heavy in our scenario. Such stop masses gives large radiative corrections to the Higgs mass, and in fact the Higgs mass is pushed up to 125GeV in sizable regions of the parameter space. The production cross section of such a lighter stop pair is comparable to those of the gluino and the squarks, and the expected number of the stops to 100fb^{-1} are between 880 and 540. Thus we can expect that the lighter stops also will be found at the 14TeV run of LHC.

The SUSY spectrum is consistent with the present results on muon anomalous magnetic moment within 3σ and $b \rightarrow s + \gamma$ and $B_s \rightarrow \mu\mu$ within 1σ . The direct detection cross section of the neutralino is from 5×10^{-47} to 10^{-47}cm^2 and is in reach of XENON 1ton and LUX/ZEP 20ton.

In conclusion, our scenario is predictive and indeed testable in the coming 14TeV LHC run. When SUSY is the solution of the lithium-7 problem and its breaking is controlled in the CMSSM framework, the time to discover SUSY is coming soon.

Acknowledgments

The work of Y.K. was financially supported by the Sasakawa Scientific Research Grant from The Japan Science Society. This work was supported in part by the Grant-in-Aid for the Ministry of Education, Culture, Sports, Science, and Technology, Government of Japan, No. 24340044 (J.S.). and No. 25003345 (M.Y.) and No. 23740190 (T.S.).

-
- [1] G. Aad *et al.* [ATLAS Collaboration], Phys. Lett. B **716** (2012) 1 [arXiv:1207.7214 [hep-ex]].
 - [2] S. Chatrchyan *et al.* [CMS Collaboration], Phys. Lett. B **716** (2012) 30 [arXiv:1207.7235 [hep-ex]].
 - [3] S. F. King and P. L. White, Phys. Rev. D **52**, 4183 (1995) [hep-ph/9505326].
 - [4] O. Buchmueller, R. Cavanaugh, A. De Roeck, M. J. Dolan, J. R. Ellis, H. Flacher, S. Heinemeyer

- and G. Isidori *et al.*, Eur. Phys. J. C **72**, 2020 (2012) [arXiv:1112.3564 [hep-ph]].
- [5] M. Kadastik, K. Kannike, A. Racioppi and M. Raidal, JHEP **1205**, 061 (2012) [arXiv:1112.3647 [hep-ph]].
- [6] Y. Okada, M. Yamaguchi and T. Yanagida, Prog. Theor. Phys. **85** (1991) 1.
- [7] J. R. Ellis, G. Ridolfi and F. Zwirner, Phys. Lett. B **257** (1991) 83.

- [8] H. E. Haber and R. Hempfling, Phys. Rev. Lett. **66** (1991) 1815.
- [9] J. A. Casas, J. R. Espinosa, M. Quiros and A. Riotto, Nucl. Phys. B **436** (1995) 3 [Erratum-ibid. B **439** (1995) 466] [hep-ph/9407389].
- [10] J. F. Navarro, C. S. Frenk and S. D. M. White, Astrophys. J. **462** (1996) 563 [astro-ph/9508025].
- [11] D. Clowe, M. Bradac, A. H. Gonzalez, M. Markevitch, S. W. Randall, C. Jones and D. Zaritsky, Astrophys. J. **648** (2006) L109 [astro-ph/0608407].
- [12] V. Springel, J. Wang, M. Vogelsberger, A. Ludlow, A. Jenkins, A. Helmi, J. F. Navarro and C. S. Frenk *et al.*, Mon. Not. Roy. Astron. Soc. **391** (2008) 1685 [arXiv:0809.0898 [astro-ph]].
- [13] M. Boylan-Kolchin, V. Springel, S. D. M. White, A. Jenkins and G. Lemson, Mon. Not. Roy. Astron. Soc. **398** (2009) 1150 [arXiv:0903.3041 [astro-ph.CO]].
- [14] Q. Guo, S. White, M. Boylan-Kolchin, G. De Lucia, G. Kauffmann, G. Lemson, C. Li and V. Springel *et al.*, Mon. Not. Roy. Astron. Soc. **413** (2011) 101 [arXiv:1006.0106 [astro-ph.CO]].
- [15] G. Hinshaw, D. Larson, E. Komatsu, D. N. Spergel, C. L. Bennett, J. Dunkley, M. R.olta and M. Halpern *et al.*, arXiv:1212.5226 [astro-ph.CO].
- [16] J. L. Feng, K. T. Matchev and T. Moroi, Phys. Rev. Lett. **84** (2000) 2322 [hep-ph/9908309].
- [17] J. L. Feng, K. T. Matchev and T. Moroi, Phys. Rev. D **61** (2000) 075005 [hep-ph/9909334].
- [18] E. Aprile *et al.* [XENON100 Collaboration], Phys. Rev. Lett. **107** (2011) 131302 [arXiv:1104.2549 [astro-ph.CO]].
- [19] O. Buchmueller, R. Cavanaugh, M. Citron, A. De Roeck, M. J. Dolan, J. R. Ellis, H. Flacher and S. Heinemeyer *et al.*, Eur. Phys. J. C **72** (2012) 2243 [arXiv:1207.7315 [hep-ph]].
- [20] K. Griest and D. Seckel, Phys. Rev. D **43** (1991) 3191.
- [21] J. Edsjo and P. Gondolo, Phys. Rev. D **56** (1997) 1879.
- [22] L. Aparicio, D. G. Cerdeno and L. E. Ibanez, JHEP **1204** (2012) 126 [arXiv:1202.0822 [hep-ph]].
- [23] M. Citron, J. Ellis, F. Luo, J. Marrouche, K. A. Olive and K. J. de Vries, Phys. Rev. D **87**, 036012 (2013) [arXiv:1212.2886 [hep-ph]].
- [24] S. Profumo, K. Sigurdson, P. Ullio and M. Kamionkowski, Phys. Rev. D **71** (2005) 023518 [arXiv:astro-ph/0410714].
- [25] T. Jittoh, J. Sato, T. Shimomura and M. Yamanaka, Phys. Rev. D **73** (2006) 055009 [arXiv:hep-ph/0512197].
- [26] K. Jedamzik, Phys. Rev. D **70**, 063524 (2004) [arXiv:astro-ph/0402344].
- [27] M. Kawasaki, K. Kohri and T. Moroi, Phys. Lett. B **625**, 7 (2005) [arXiv:astro-ph/0402490].
- [28] M. Kawasaki, K. Kohri and T. Moroi, Phys. Rev. D **71**, 083502 (2005) [arXiv:astro-ph/0408426].
- [29] M. Pospelov, Phys. Rev. Lett. **98**, 231301 (2007) [arXiv:hep-ph/0605215].
- [30] K. Kohri and F. Takayama, Phys. Rev. D **76**, 063507 (2007) [arXiv:hep-ph/0605243].
- [31] M. Kaplinghat and A. Rajaraman, Phys. Rev. D **74**, 103004 (2006) [arXiv:astro-ph/0606209].
- [32] R. H. Cyburt, J. R. Ellis, B. D. Fields, K. A. Olive and V. C. Spanos, JCAP **0611**, 014 (2006) [arXiv:astro-ph/0608562].
- [33] K. Hamaguchi, T. Hatsuda, M. Kamimura, Y. Kino and T. T. Yanagida, Phys. Lett. B **650** (2007) 268 [arXiv:hep-ph/0702274].
- [34] C. Bird, K. Koopmans and M. Pospelov, Phys. Rev. D **78**, 083010 (2008) [arXiv:hep-ph/0703096].
- [35] M. Kawasaki, K. Kohri and T. Moroi, Phys. Lett. B **649**, 436 (2007) [arXiv:hep-ph/0703122].
- [36] T. Jittoh, K. Kohri, M. Koike, J. Sato, T. Shimomura and M. Yamanaka, Phys. Rev. D **76** (2007) 125023 [arXiv:0704.2914 [hep-ph]].
- [37] K. Jedamzik, Phys. Rev. D **77**, 063524 (2008) [arXiv:0707.2070 [astro-ph]].
- [38] D. Cumberbatch, K. Ichikawa, M. Kawasaki, K. Kohri, J. Silk and G. D. Starkman, Phys. Rev. D **76**, 123005 (2007) [arXiv:0708.0095 [astro-ph]].
- [39] J. Pradler and F. D. Steffen, Phys. Lett. B **666**, 181 (2008) [arXiv:0710.2213 [hep-ph]].
- [40] M. Kawasaki, K. Kohri, T. Moroi and A. Yotsuyanagi, Phys. Rev. D **78**, 065011 (2008) [arXiv:0804.3745 [hep-ph]].
- [41] T. Jittoh, K. Kohri, M. Koike, J. Sato, T. Shimomura and M. Yamanaka, Phys. Rev. D **78** (2008) 055007 [arXiv:0805.3389 [hep-ph]].
- [42] M. Kusakabe, T. Kajino, T. Yoshida, T. Shima, Y. Nagai and T. Kii, Phys. Rev. D **79**, 123513 (2009) [arXiv:0806.4040 [astro-ph]].
- [43] M. Pospelov, J. Pradler and F. D. Steffen, JCAP **0811**, 020 (2008) [arXiv:0807.4287 [hep-ph]].
- [44] M. Kamimura, Y. Kino and E. Hiyama, Prog. Theor. Phys. **121**, 1059 (2009) [arXiv:0809.4772 [nucl-th]].
- [45] K. Kohri and Y. Santoso, Phys. Rev. D **79**, 043514 (2009) [arXiv:0811.1119 [hep-ph]].
- [46] S. Bailly, K. Jedamzik and G. Moulataka, Phys. Rev. D **80**, 063509 (2009) [arXiv:0812.0788 [hep-ph]].
- [47] S. Bailly, K. Y. Choi, K. Jedamzik and L. Roszkowski, JHEP **0905**, 103 (2009) [arXiv:0903.3974 [hep-ph]].
- [48] R. H. Cyburt, J. Ellis, B. D. Fields, F. Luo, K. A. Olive and V. C. Spanos, JCAP **0910**, 021 (2009) [arXiv:0907.5003 [astro-ph.CO]].
- [49] T. Jittoh, K. Kohri, M. Koike, J. Sato, T. Shimomura and M. Yamanaka, Phys. Rev. D **82** (2010) 115030 [arXiv:1001.1217 [hep-ph]].
- [50] M. Kusakabe, T. Kajino, T. Yoshida and G. J. Mathews, Phys. Rev. D **81**, 083521 (2010) [arXiv:1001.1410 [astro-ph.CO]].
- [51] M. Pospelov and J. Pradler, Phys. Rev. D **82**, 103514 (2010) [arXiv:1006.4172 [hep-ph]].
- [52] M. Pospelov and J. Pradler, Ann. Rev. Nucl. Part. Sci. **60** (2010) 539 [arXiv:1011.1054 [hep-ph]].
- [53] M. Kawasaki and M. Kusakabe, Phys. Rev. D **83**, 055011 (2011) [arXiv:1012.0435 [hep-ph]].
- [54] T. Jittoh, K. Kohri, M. Koike, J. Sato, K. Sugai, M. Yamanaka and K. Yazaki, Phys. Rev. D **84** (2011) 035008 [arXiv:1105.1431 [hep-ph]].
- [55] M. Kusakabe, A. B. Balantekin, T. Kajino and Y. Pehlivan, Phys. Lett. B **718** (2013) 704 [arXiv:1202.5603 [astro-ph.CO]].
- [56] K. Kohri, S. Ohta, J. Sato, T. Shimomura and M. Yamanaka, Phys. Rev. D **86** (2012) 095024 [arXiv:1208.5533 [hep-ph]].
- [57] M. Kusakabe, K. S. Kim, M. -K. Cheoun, T. Kajino and Y. Kino, arXiv:1305.6155 [astro-ph.CO].
- [58] L. Monaco, P. Bonifacio, L. Sbordone, S. Villanova and E. Pancino, Astron. Astrophys. **519** (2010) L3. [arXiv:1008.1817 [astro-ph.GA]].
- [59] A. Coc, S. Goriely, Y. Xu, M. Saimpert and E. Vangioni, Astrophys. J. **744** (2012) 158 [arXiv:1107.1117 [astro-ph]].

- ph.CO]].
- [60] F. Spite and M. Spite, *Astron. Astrophys.* **115** (1982) 357.
 - [61] [CMS Collaboration], CMS-PAS-HIG-12-045. ATLAS:2012klqCMS:aya
 - [62] [ATLAS Collaboration], ATLAS-CONF-2012-170.
 - [63] B. C. Allanach, *eConf C* **010630**, P319 (2001) [hep-ph/0110227].
 - [64] A. Djouadi, hep-ph/0211357.
 - [65] B. C. Allanach, S. Kraml and W. Porod, *JHEP* **0303**, 016 (2003) [hep-ph/0302102].
 - [66] B. C. Allanach, A. Djouadi, J. L. Kneur, W. Porod and P. Slavich, *JHEP* **0409**, 044 (2004) [hep-ph/0406166].
 - [67] G. Belanger, F. Boudjema, A. Pukhov and A. Semenov, arXiv:1305.0237 [hep-ph].
 - [68] W. Porod, *Comput. Phys. Commun.* **153** (2003) 275 [hep-ph/0301101].
 - [69] W. Porod and F. Staub, *Comput. Phys. Commun.* **183** (2012) 2458 [arXiv:1104.1573 [hep-ph]].
 - [70] S. Heinemeyer, W. Hollik and G. Weiglein, *Comput. Phys. Commun.* **124** (2000) 76 [hep-ph/9812320].
 - [71] S. Heinemeyer, W. Hollik and G. Weiglein, *Eur. Phys. J. C* **9** (1999) 343 [hep-ph/9812472].
 - [72] G. Degrandi, S. Heinemeyer, W. Hollik, P. Slavich and G. Weiglein, *Eur. Phys. J. C* **28** (2003) 133 [hep-ph/0212020].
 - [73] M. Frank, T. Hahn, S. Heinemeyer, W. Hollik, H. Rzehak and G. Weiglein, *JHEP* **0702** (2007) 047 [hep-ph/0611326].
 - [74] S. P. Martin, In *Kane, G.L. (ed.): Perspectives on supersymmetry II* 1-153 [hep-ph/9709356].
 - [75] J. Pradler and F. D. Steffen, *Nucl. Phys. B* **809**, 318 (2009) [arXiv:0808.2462 [hep-ph]].
 - [76] S. Chatrchyan *et al.* [CMS Collaboration], arXiv:1305.0491 [hep-ex].
 - [77] [ATLAS Collaboration], ATLAS-CONF-2013-037 .
 - [78] G. W. Bennett *et al.* [Muon G-2 Collaboration], *Phys. Rev. D* **73** (2006) 072003 [hep-ex/0602035].
 - [79] K. Hagiwara, R. Liao, A. D. Martin, D. Nomura and T. Teubner, *J. Phys. G* **38** (2011) 085003 [arXiv:1105.3149 [hep-ph]].
 - [80] RAaij *et al.* [LHCb Collaboration], *Phys. Rev. Lett.* **110** (2013) 021801 [arXiv:1211.2674 [hep-ex]].
 - [81] Y. Amhis *et al.* [Heavy Flavor Averaging Group Collaboration], arXiv:1207.1158 [hep-ex].
 - [82] J. beringer *et al.* [Particle Data Group Collaboration], *Phys. Rev. D* **86** (2012) 010001
 - [83] G. Jungman, M. Kamionkowski and K. Griest, *Phys. Rept.* **267** (1996) 195 [hep-ph/9506380].
 - [84] E. Aprile *et al.* [XENON100 Collaboration], *Phys. Rev. Lett.* **109** (2012) 181301 [arXiv:1207.5988 [astro-ph.CO]].
 - [85] E. Aprile [XENON1T Collaboration], arXiv: 1206.6288 [astro-ph.IM].
 - [86] D. S. Akerib *et al.* [LUX Collaboration], *Astropart. Phys.* **45** (2013) 34 [arXiv:1210.4569 [astro-ph.IM]].
 - [87] A. Belyaev, N. D. Christensen and A. Pukhov, *Comput. Phys. Commun.* **184** (2013) 1729 [arXiv:1207.6082 [hep-ph]].